

5.

EVALUATION OF INVERSE METHODS AND HEAD MODELS FOR EEG SOURCE LOCALIZATION USING A HUMAN SKULL PHANTOM



TOCCARE

Résumé — Cette étude concerne l'évaluation de la précision de diverses méthodes d'inversion pour le problème de la localisation de sources de l'EEG. Pour un meilleur réalisme de la simulation des conditions d'enregistrement des signaux, nous avons utilisé un montage expérimental avec des sources de courant positionnées à l'intérieur d'un crâne humain rempli d'un milieu conducteur. Les performances respectives de méthodes de fit spatio-temporel de dipôle et de celles basées sur des modèles de sources distribuées dans le volume intra crânien ou sur la surface corticale sont évaluées. Nous traiterons particulièrement de l'influence des solutions du problème direct sur la précision localisatrice des méthodes inverses. Ainsi, nous considérerons des modèles de tête allant de la sphère homogène par morceaux à un modèle de tissus anisotropes réalisé avec la méthode des éléments finis, en passant par un modèle homogène par morceaux et à géométrie réaliste.

Nos résultats indiquent que les erreurs issues d'un modèle de fit dipolaire spatio-temporel sont dans l'intervalle de 6 à 20mm avec un taux de variance résiduelle très élevé. Quant aux méthodes à base de sources distribuées sur la surface corticale, celles-ci sont à même de localiser la source active avec presque toujours une très bonne précision, avec peu ou pas d'activité parasite, et ce, même lorsque deux sources sont actives simultanément. Nous en concluons que lorsqu'un petit nombre de sources focales sont activées, les détails de la géométrie crânienne ainsi que les propriétés de conduction des tissus n'influencent que très peu la localisation des sources originales lorsque des méthodes de régularisation adaptées sont utilisées dans la résolution du problème inverse.

Abstract — The present study investigates the accuracy of various inverse methods in the EEG source localization problem. For increased realism in the simulation of the recording conditions of brain waves, we have used a montage with current sources located at various positions and orientations inside a human skull filled with a conductive medium. The respective merits of methods based on spatio-temporal dipole fit or source models distributed in the whole head volume or on the cortical surface are then evaluated. We particularly refer to the influence of the solution to the forward problem on the localization accuracy of inverse methods. Thus, head models ranging from the piece-wise homogeneous sphere, the piece-wise homogeneous model with realistic geometry computed with the Boundary Element Method, to the anisotropic model computed with the Finite Element Method are considered.

Results indicate that localization errors of a spatio-temporal dipole fit in the head volume with the sphere model are on the range of 6 to 20mm with high rates of residual variance in the data. Further, in this study, inverse methods that take the cortical anatomy into account are almost always able to locate with great precision the active source, with no or little spurious activity in close or distant regions, even when 2 sources are simultaneously active. We report that when few focal areas are active, the fine head geometry and the conductivity properties of the head tissues may little influence the estimation of the active zones, if proper regularization schemes are used for the processing of the inverse problem.

Keywords — EEG, source localization, inverse problem, phantom, boundary element method, finite element method.

1. INTRODUCTION

Recent developments in the instrumentation of EEG and MEG now allow the simultaneous recording of the scalp electric potentials and magnetic fields with entire head coverage. This new generation of devices participates to the enthusiasm in both the Medical Imaging and Cognitive Neuroscience research communities which tend to make EEG and MEG become genuine functional brain imaging modalities with high temporal resolution (Wikswa *et al.* 1993, Gevins 1998).

Imaging the electrical activity of the brain during sensory-motor or cognitive tasks consists in estimating the underlying sources of the EEG and/or the MEG recordings in space and time. We would like to briefly recall the basics of such source estimation.

First, a proper physical model for the neural current sources is needed. The widely used current dipole is considered as a correct approximation of the synchronous activation of a population of about 10^6 cortical macro-columns of pyramidal cells (Hämäläinen *et al.* 1983, Gloor 1985, Nunez 1981). Second, a physical description of the production of the brain electrical potentials and magnetic fields outside the head is given by the solution to the forward problem. This procedure consists in computing the unit response of the sensor array for any possible source location and orientation. Thus, this computation necessitates taking into account both the head geometry and the conductivity properties of the head tissues. The head geometry may be basically approximated by a set of concentric spheres with homogeneous conductivity properties. Here, analytical computation of potentials and fields are possible (Sarvas 1987, de Munck 1992). Increased realism in the model of the head geometry can be achieved with a tessellation of the head compartments from anatomical MRI images. Piece-wise homogeneous head models are obtained from surface meshes and the forward problem is solved with the Boundary Element Method (BEM) approach (Meijs *et al.* 1989). Anisotropy properties of tissue conductivity can be taken into account owing to volume meshes with tetrahedrons and the application of the Finite Element Method (FEM) to the forward procedure (Haueisen *et al.* 1995, Marin *et al.* 1998).

Then, inverse procedures consist in estimating the underlying source pattern given one of the previous head models and a certain time window of interest. One salient point here is that inverse procedures are dedicated to work in connection with a head model which is, whatever its degree of realism may be, a simplified description of the complex arrangement of head tissues.

Moreover, as long as no *in vivo* method for the measure of conductivity properties is available, even the FEM models with anisotropy parameters will still assume the common average values that have been measured on dead tissues (Rush & Driscoll 1968, Robillard & Poussart 1977).

Thus, it is necessary to investigate whether an inverse procedure may be able to overcome the systematic bias of the forward solution for reliable localization of brain sources. Numerical solutions to the forward problem have been evaluated in comparison to analytical solutions in the sphere case (see Marin *et al.* 1998 and Thévenet *et al.* 1991 for instance). Further, the influence of head geometry and the conductivity of tissues on scalp potentials and magnetic fields have been also widely investigated (Haueisen *et al.* 1995, Marin *et al.* 1998). However, little has been done for the evaluation of the systematic bias introduced by both the head model and the source priors used in the inverse procedure, and their influence on the accuracy of source localization (Miltner *et al.* 1994, Yvert *et al.* 1997).

Moreover, most of the numerous source localization methods that are now available have been evaluated in the simplified context of noisy simulations assuming white Gaussian additive noise on sensors. This model does not reflect properly the large range of possible correlated perturbations between sensors like head model bias, and of course environment noise or brain background activity.

One possible way to achieve increased realism in the evaluation and the validation of inverse methods consist in operating physical simulations of EEG or MEG recordings. The first approach in this field consisted in recording the EEG induced by dipolar sources simulated owing to electrodes implanted in epilepsy patients for pre-surgery monitoring (Cohen *et al.* 1990). An interesting system for more systematic studies with greater freedom in the arrangement of the source positions and firings, is the phantom head. The simplest systems of that kind have been using a uniform and non-conductive medium for the evaluation of inverse methods with MEG (cf. Phillips *et al.* 1997 for instance). Further, as the evaluation of BEM or FEM models with realistic geometry necessitates the generation of volume currents, several MEG studies have been using cadaver heads (Barth *et al.* 1996) or non-conductive media to approximate the shape of the human skull filled with some saline solutions (Greenblatt and Robinson 1994, Mennighaus *et al.* 1994, Lewine *et al.* 1995).

If EEG recordings are required, it is necessary to use a conductive medium for the skull compartment too. In (Leahy *et al.* 1998), a joint MEG and EEG study with a human skull phantom is described for the investigation of the localization accuracy of the R-MUSIC method (Mosher & Leahy, 1998) with both spherical and BEM head models. In (Baillet *et al.* 1997), we present an EEG experiment with a similar human skull phantom head for the evaluation of the sphere, BEM and anisotropic FEM solutions to the forward problem.

The present article is a companion study to (Baillet *et al.* 1997) for the localization accuracy of different approaches to the EEG inverse problem. We propose here to investigate the reliability of several inverse methods, from the spatio-temporal dipole fit to the distributed source models on the cortex, when using the complete range of head models, from the sphere to anisotropic FEM (after measurement of the conductivity values of the phantom head tissues).

In section 2 of this report, we quickly recall the experimental setting and the conductivity properties of the phantom head. In this section, we then present the different head models that have been used in the inverse procedures. The results regarding the localization accuracy are then presented in section 3. In section 3.1, the popular spatio-temporal dipole fit with BESA (Neuroscan Inc.) are presented and discussed. In section 3.2, we evaluate the solutions descending from source models distributed through the whole head volume with the LORETA (Pascual-Marqui *et al.* 1994) method. In section 3.3, the source space is then distributed on a simulated cortical surface and we present the results obtained from Minimum Norm Estimates (MNE) of the source activity, recursive and weighted focusing of MNE (FOCUSS, Gorodinsky *et al.* 1995), and the non-linear ST-MAP method (Baillet & Garnero 1997). Finally, we draw some conclusions in section 5.

2. EXPERIMENTAL MATERIALS AND PHYSICAL MODELS.

2.1 THE EXPERIMENTAL SETTING

2.1.1 THE HUMAN SKULL PHANTOM HEAD

The phantom head is made of a dry human skull filled with solidified saline gelatin. 6 current sources made of semi-rigid coaxial cables embedded in thin glass tubes ($1.5mm$, outer diameter) are brought into the inner volume via the occipital hole. The glass tubes allow a precise and stable positioning of the dipoles during the experiment. Every dipole is fed owing to an independent current source that is optically isolated to avoid current leakage. The maximum current value is set to $2mA$ for a dipole length of $7mm$, thus producing an equivalent current dipole of maximum moment $14nA.m$. The source signal for every dipole is independently stored in

EPROM's after coding in 12 bits words and sent to the current source at a sample rate of 10,000 words per second (cf. Baillet *et al.* 1997 for more details).

2.1.2 DATA ACQUISITION

The sensor array consisted of a cap of 60 electrodes uniformly distributed over the scalp surface. The recording sampling rate has been set to $1kHz$. The current signal was the same for every source, and corresponded to a damped sinusoidal time course with $10Hz$ frequency and $600ms$ length, following a $150ms$ blank interval for noise measurement. Every EEG recording has been scheduled with 15 trials synchronized on a TTL-compatible signal out of the source driver electronics. During the experiment, every single and every possible pair of sources have been recorded one after the other.

2.2 REGISTRATION IN A SINGLE COORDINATE SYSTEM

The electrode positions, the source locations and orientations, and finally the global head shape have been registered in a single coordinate system after CT Scan acquisition of the whole head volume (145 slices, $1mm$ thickness). This global approach reduces the possible registration errors, as a single coordinate system is being used. Figure 1 shows a typical slice of the CT Scan with a 3D reconstruction of the electrode and the sources in their positioning tubes.

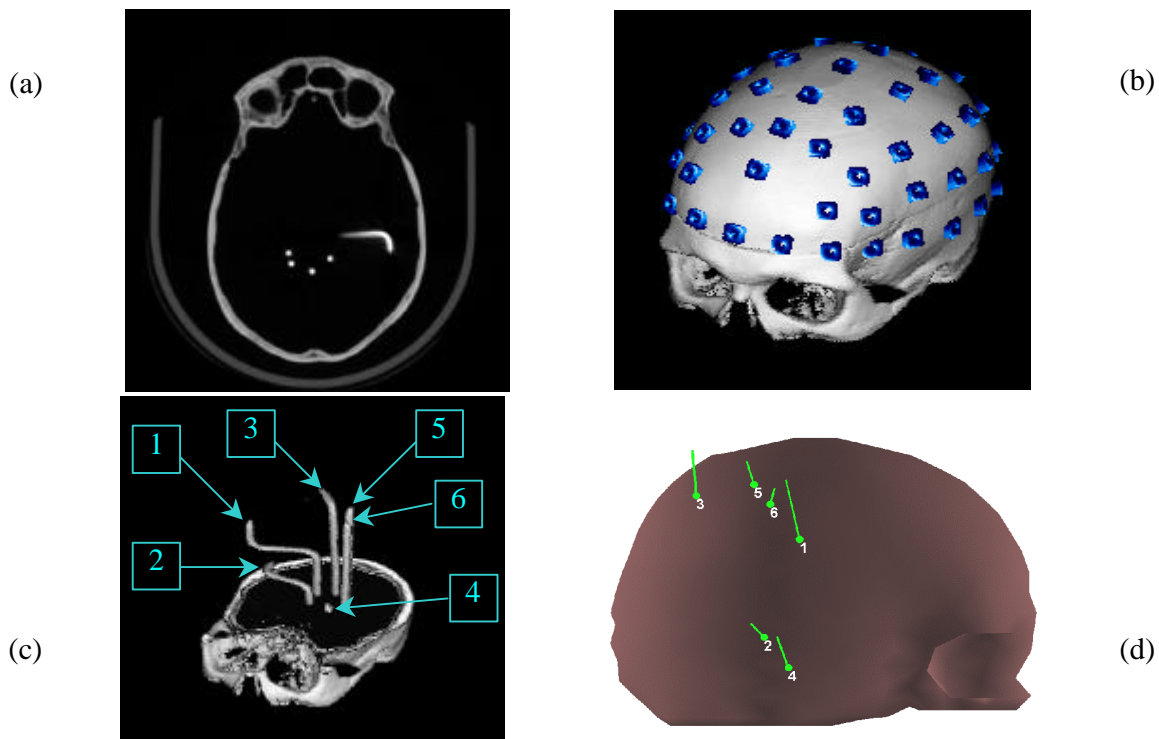


Figure 1 — The phantom head: (a) a typical slice of the CTScan, a source cable is visible on the picture; (b) a 3D view of the coregistered 60 electrode array on the skull; (c) a 3D view of the sources with their corresponding positioning tubes; (d) a right side view of the 6 dipole sources, after registration with the CTScan coordinate system.

2.3 MEASUREMENT OF THE CONDUCTIVITY PROPERTIES

As we aim at evaluating the respective merits of different head models on the localization accuracy of inverse procedures, we have designed several head models of the phantom head with increasing degree of realism (cf. section 2.4 below). The simplest model will be a 2-concentric spheroidal model of the phantom head, while the most complex one will take into account the true head geometry and the anisotropic conductivity properties of the skull. We recall in Table 1 the conductivity measures that we have obtained and extensively described in (Baillet *et al.* 1997).

	<i>Skull Thickness</i> (mm)	<i>Tangential</i> <i>Conductivity (S)</i>	<i>Radial</i> <i>Conductivity (S)</i>	<i>Saline Gelatin</i> <i>Conductivity (S)</i>
<i>Average</i>	6.05	0.0107	0.0140	
<i>Minimum</i>	3.8	0.0035	0.0075	1.11
<i>Maximum</i>	11	0.0352	0.03	
<i>Standard</i> <i>Deviation</i>	1.45	0.0065	0.0071	

Table 1 — Summary of measurements for skull geometry and conductivity. The average conductivity values are computed on 29 measurement points over the scalp surface

The average ratio between skull conductivity and gelatin is about 1/90, which is extremely consistent with the values that are usually assumed for real head tissues (see for instance (Peters & de Munck 1990) (1/40), (Rush & Driskoll 1968) (1/80), (Cuffin 1990) (1/80.5)).

2.4 SOLUTIONS TO THE FORWARD PROBLEM

In the present work, we will refer to 5 different head models, with increasing degree of realism. These are the following (the corresponding acronyms are written in Italics):

Anisotropic and heterogeneous model using FEM (*FEManiso*): After surface segmentation, the 3D mesh with tetrahedrons has been designed with the I-DEAS VI.i software (SDRC Company) (Marin *et al.* 1998). The average size of the mesh element is 9mm. Then, the measured conductivity values have been introduced in this anisotropic model after interpolation over the whole skull surface, for both tangential and radial conductivity. This step leads to the constitution of a conductivity tensor that can be taken explicitly into account

by the FEM formulation. The Maxwell equations have been solved with the FEM code of the Flux3D Software (Cédrat Company, France), cf. Figure 2.

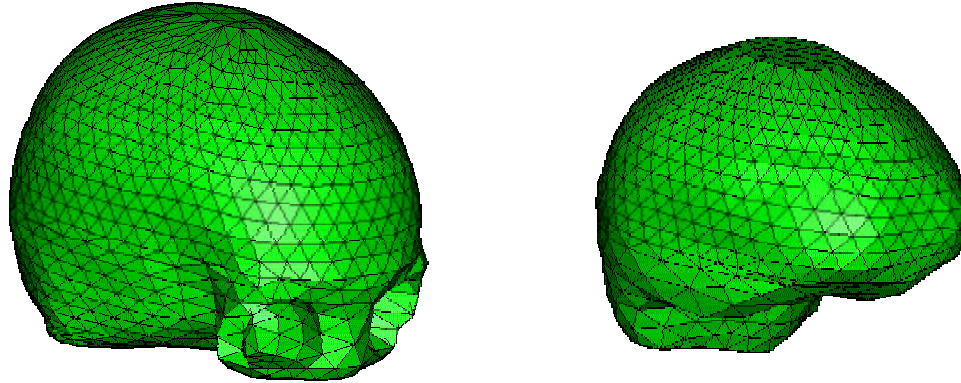


Figure 2— The 3D mesh of the Phantom Head : Left, outer surface (skull volume 7694 elements);
Right, inner volume (“brain” volume 13067 elements).

- Homogeneous and anisotropic model using FEM (*FEManiso_TR*) : This model is a simplified version of *FEManiso* where the skull is considered as homogeneous with anisotropy conductivity properties reduced to the average tangential and radial conductivity values (0.0140 S and 0.0107 S respectively). This model will be useful to check whether heterogeneity of the conductivity properties of the skull is likely to play an important role in the localization accuracy. Please note a ratio of 1/10 can be achieved between the minimum and maximum tangential conductivity values of the skull (cf. Table 1).
- Homogeneous and Isotropic Model using FEM (*FEMiso*): This is the simplest model with realistic geometry that can be obtained with FEM. The respective conductivity values for the brain volume and the skull have been set to the average conductivity values: 1.11 S and 0.0125 S respectively. This later is the average value between tangential and radial conductivity of the skull.
- Piece-wise homogeneous model with realistic geometry and BEM computation with linear interpolation (*BEM*): The associated surface tessellation has been designed from the volume mesh. The triangles are parts of the tetrahedrons that intersect the volume surfaces between the brain and the inner/outer skull surface respectively. BEM models now become more and more popular with significant simplification of the computation in comparison to FEM but do not authorize the introduction of anisotropy of the conductivity properties.

- Piece-wise homogeneous n -concentric sphere model (*Sphere*): this is the most widely used geometry because it does not necessitate any MRI or CTScan examination for anatomical registration with EEG. The electrodes can be located owing to a 3D-digitalization device (3D Isotrack, Polhemus). Further, the forward problem can be solved owing to an analytical expression of the potentials on the scalp (de Munck 1988). Here, a 2-concentric sphere model that approximates the inner and outer skull surfaces has been fitted to the phantom head. As no scalp surface has been designed for the phantom head, this spherical model is the simplified version of the well-known 3-sphere head model. Nevertheless the phantom head properly models the main conductivity edge between the brain and the skull, which is primarily responsible for the attenuation and the diffusion of the volume currents at the surface of the head. The respective radii of the sphere for inner and outer skull are $8.17cm$ and $9.11cm$.

These head models are now used with a set of different inverse procedures to estimate their ability to recover the focal dipolar sources of the phantom head, and their sensitivity to approximation in the head modelization.

2.5 PHANTOM "EVOKED POTENTIALS"

The inverse methods have been tested on a set of simulated evoked potentials (EP's) generated by averaging 15 EEG sequences of $800ms$ for every single dipole (source $n^{\circ}1$ to $n^{\circ}6$, which will be denoted S1 to S6). Figure 3 shows one EP time course of the potentials and the corresponding scalp topography at the 210ms-peak (S1). After averaging, the amount of noise

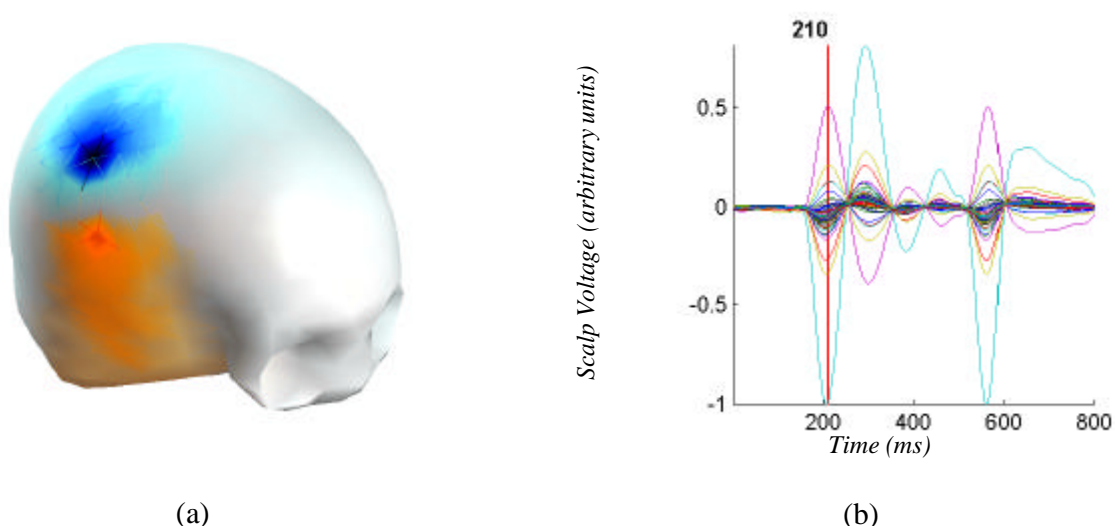


Figure 3 — A typical EEG topography on the phantom head after averaging over 15 trials.
 (a) Potential map interpolated between the 60 electrodes for source S1, time 210ms ;
 (b) the corresponding superimposed signals on the 60 electrode set (average referenced).

appeared to be insignificant in the data for every source (and notably during the “silent” interval before activation of a current source). Thus, this data set is well adapted to the study of the influence of the head model only, on the accuracy of inverse procedures.

3. ESTIMATION OF THE LOCALIZATION ACCURACY OF TYPICAL INVERSE PROCEDURES

We have chosen a typical set of inverse procedures, ranked accordingly to an increasing amount of *a priori* information regarding the source space.

3.1 SPATIO-TEMPORAL DIPOLE FIT

3.1.1 BASICS OF THE DIPOLE FIT METHODS

Basically, the first inverse procedures to appear are the so-called dipole fit methods that search for the best dipole position(s) and orientation(s) to explain the data. For a certain number of dipoles given *a priori*, the estimation is guided by non-linear minimization of a cost function. Dipoles may be fitted sequentially for different time points of interest of the EEG scalp topography (Snyder 1991), or by taking into account the spatio-temporal evolution of the signal on a given time window. This later approach belongs to the family of spatio-temporal dipole modeling. The non-linear optimization techniques range from gradient (see for instance Marquardt 1963) and downhill simplex search methods (Huang *et al.* 1998), but also Simulated Annealing (Haneishi *et al.* 1994, Khosla *et al.* 1997). This later approach has been proposed to overcome the sensitivity of the deterministic algorithms to initial conditions. Actually, when the number of unknown parameters grows, the solutions proposed by deterministic least-square fits tend to get trapped in some local minima of the cost function. Thus, the final result is extremely dependent on the quality of the initial guess regarding the number of dipoles to estimate and their initial locations and orientations. Very often, application of these methods are limited to spherical head models for fast calculation of the forward solution for a given dipole position and orientation. Nevertheless, single dipole fits with realistic head models now tend to be used on inter-ictal source localization in epilepsy (Roth *et al.* 1997).

Dipole fit methods and more particularly the BESA implementation from Scherg (Brain Electrical Source Analysis software (Neuroscan Inc.)) have proved to be powerful exploration tools for many cognitive and clinical studies, see for instance (Scherg and Von Cramon, 1986), (Ebersole, 1994). As mentioned above, practical implementations of dipole fit methods are very sensitive to initial guess of both the number and the location of the underlying sources, but they are also really dependent on the degree of experience the user has on EP data for instance. Important questions like “*how many dipoles should be chosen at the beginning ?*”, “*how to build the cost function ?*”, “*should we choose moving or fixed dipole orientations ?*”, and to “*which extent the source estimate should fit to the data ?*” are soon to appear when trying to explain a certain scalp topography.

An interesting study with simulated EP data has dealt with the estimation of the influence of the user on the source localization accuracy with BESA (Miltner *et al.* 1994). It is shown that the grand-average location error on 9 subjects who were familiar with EP data is *1.4cm* with a standard deviation of *1.0 cm*. This study confirmed that the accuracy of the source localization especially depends on the number of underlying sources and their relative locations, orientations and temporal overlapping. Further, some sources may not be present in the final estimate while they were in the real data. However, the simulated data set was made of a complex sequence of 10 sources, with both successive and overlapping activities. But here, the simulated EEG was generated through the same spherical head model as the one used during the source localization. Thus, no conclusion could be driven from the possible bias induced by simplifications of the head model.

3.1.2 BASICS OF BESA

The BESA source modeling considers a set of consecutive time points to fit a dipole configuration that is supposed to be stable in location with fixed or varying orientation. After a time window of interest has been chosen from the data (and especially the scalp topography), it is first necessary to give a guess of the number of underlying sources to be fitted to the data. The source estimation is then guided through the minimization of a cost function that is a weighted combination of 4 fit criteria, those are:

- 1) A criterion of Residual Variance (RV) in the data: this is the amount of signal that remains unexplained on the given time window of fit by the current source model. This criterion is defined as the following ratio:

$$RV = 100 \times \frac{\langle \langle \| V(:,t) - \hat{V}(:,t) \| \rangle \rangle}{\langle \langle \| V(:,t) \| \rangle \rangle} (\%) \quad (1)$$

Where $V(:,t)$ are the measured potentials at instant t , $\hat{V}(:,t)$ are the reconstructed potentials for a given source model according to the spherical model of the head, and $\langle \langle \| a(t) \| \rangle \rangle$ is the time average of the 2-norm of the time-varying vector $a(t)$.

2) A variance criterion that increases when the sources tend to be active outside of their *a priori* time interval of activation.

3) An energy criterion that avoids the interaction between two sources when a large amplitude of the waveform of one source is compensated by a large amplitude on the waveform of the second source, giving rise to small amplitude on the surface of the scalp.

4) A separation criterion that encourages solutions in which as few sources as possible are simultaneously active.

3.1.3 SETTING THE PARAMETERS

The BESA user who has been recruited here for the processing of the phantom data could be considered as an *omniscient* expert of phantom EP's. Actually, for every data file, he knew that only one source was active, and further, where it was approximately located. In other words, the *a priori* knowledge brought by the expert here is much more accurate than the one inferred during usual experiments of neuropsychology from:

The experimental design and paradigm (like the nature of the stimulus for instance);

The raw chronometry of events: (like "recognizing known faces shuffled into a set of unknown faces *then* push the left button");

The cognitive models that gathers the hypothesis to be tested in the current experiment;

Previous results from similar experimental protocols with the same or other functional imaging modalities.

Moreover, the real electrode locations have been used owing to the possibility offered by BESA to fit them on an ellipsoid that will then be deformed to a sphere (Figure 2). The sources

are fitted in the spherical model, then their coordinates are transformed back in the electrode

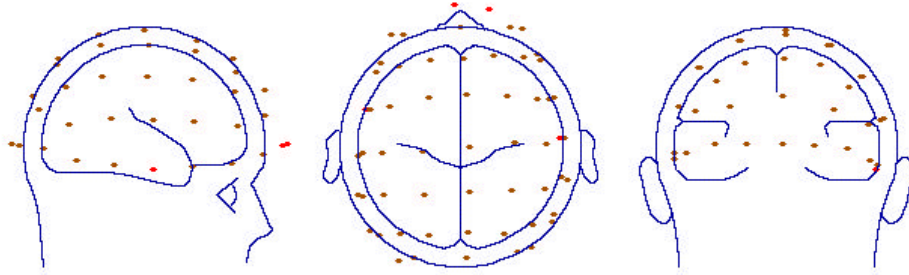


Figure 2 — Fit of the original electrode locations on the BESA spherical head model

coordinate system (*i.e.* the original CTScan/source coordinate system).

For increased realism in the dipole fit, the physical parameters of the sphere have been changed to remain as close as possible to reality. Actually, as no 2-concentric sphere is available in BESA, we have used a 3-sphere model with minimum scalp thickness (0.5mm). Bone thickness has been set to 6.05mm, which is the average skull thickness measured on the phantom. Finally, the average conductivity values have been introduced in the sphere model and set to $1.11\ S$ for brain and skin, and to $0.0125\ S$ for the skull.

In conclusion, the dipole fit has been done with the best sphere model and a user who knows exactly what he is looking for. It is then possible to discuss the performances of the spatio-temporal dipole fit for the estimation of focal sources, and the influence of the systematic bias induced by the simplified geometry and conductivity parameters of the sphere model.

3.1.4 RESULTS

The first approach consisted in fitting the best dipole source that would account for the data in the sense of the minimum RV. This technique might seem attractive but is in fact really hazardous. Actually, if the signal level is larger on a small set of electrodes (on 2 or 3 close sensors for instance) than on the rest of the sensor array, then the source estimation based on RV will only tend to fit with priority to the signal on these electrodes. The RV criterion will give little credit to the rest of the sensors as they quantitatively have little contribution to the global signal power, but unfortunately may be important for the detailed description of the potential scalp topography.

These solutions will thus produce excellent fit to the small group of electrodes that contains the maximum signal power, and consequently, the RV will have extremely small values (especially when there is only one underlying shallow source that produces little smearing of the potentials on the scalp). This dipole fit according to only 2 or 3 electrodes is in a way a reduction

of the number of data. This is equivalent to considering the signals on most of the electrodes as too noisy and it will finally increase the ambiguity of dipole localization. Further, minimum RV source models will tend to explain *too well* the data, without considering the bias introduced by the simplified head model.

Scalp potential maps, as they take all the sensors into account, are a good way to estimate whether minimum RV solutions may be trusted by visualizing the topography of the reconstructed potential maps on the scalp and comparing them to the original ones. Fortunately, over-fitted solutions tend to produce potential mapping on the scalp that may be very far from the original one, which could give an index of the poor accuracy of the current solution.

In our experiment, the spatio-temporal dipole has been fitted around the *210ms* peak, on a *50ms* time window (*[180,230] ms*). If the only fit criterion is RV, a single dipole source can explain up to more than 99% of the total signal power, but with poor localization accuracy (errors up to more than *3cm* could be encountered).

The results presented herein have been computed by minimization of a weighted combination of the available criteria described above. We gave 0% ratio to the Energy criterion as we intended to fit a single dipole; 40% to the Variance criterion, to help minimization to find a source that is active on the given time window; and 50% to the Separation criterion because it encourages solutions with few sources. Thus, only 10% credit is accorded to the RV criterion.

The results are summarized in Table 2.

	<i>Localization Error (mm)</i>	<i>Residual Variance</i>
S1	11.9	29.2 %
S2	12.8	32.8 %
S3	13.4	71.8 %
S4	19.4	29.7 %
S5	6.7	11.1 %
S6	10.6	14.1 %
Average	12.5	31.5 %

Table 2 — Spatio-temporal dipole fit with the best sphere model: localization accuracy and residual signal power that remains unexplained

The localization accuracy is on the order of *12mm*, and can be considered as the best performance that is liable to be achieved given these data and the *a priori* knowledge that has been introduced prior to dipole fitting. The average localization error is sensibly larger than the one achieved by the R-MUSIC algorithm on similar phantom data in (Leahy *et al.* 1998): *8mm*

with a spherical head model. But in this latter study, the placement of the 64 electrodes was optimized with denser spatial sampling over the dipole sources.

The original and estimated source positions and orientation are shown in Figure 3.

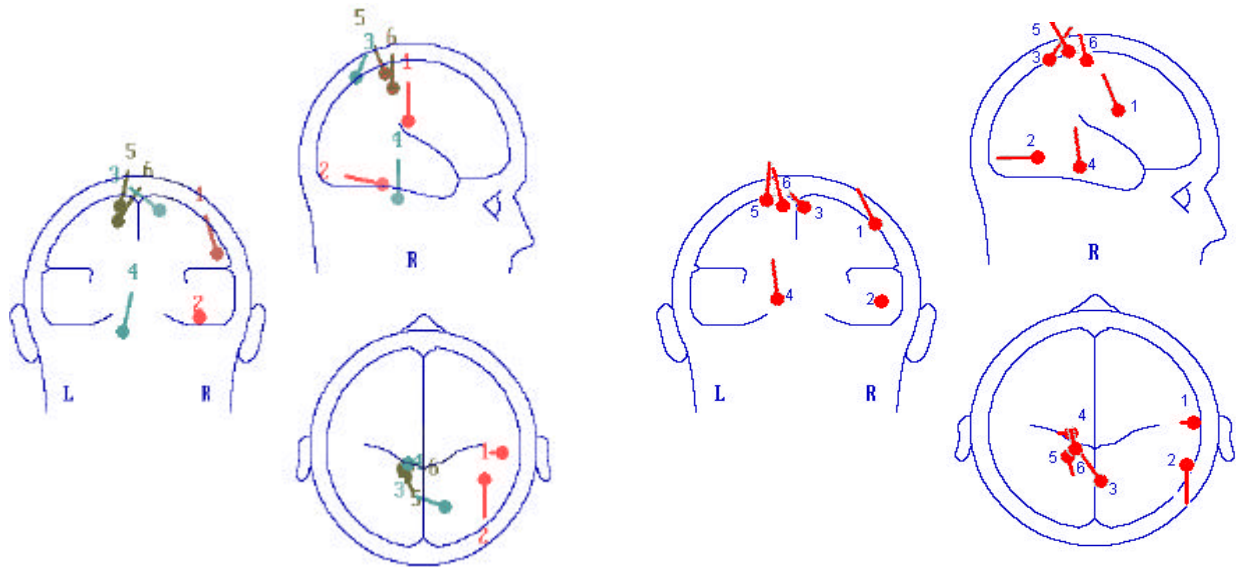


Figure 3 — The original dipole configuration in the BESA representation (left) ; the estimated dipole locations (right).

From Figure 3, it is clear that the orientations of the dipoles are almost all correctly estimated while the localization errors, though not dramatic, may perhaps be critical for precise anatomical localization when explaining real EP data sets.

The main point on which we want to stress is that while the average RV values are important, the user tried to achieve the best localization accuracy. It indicates that the spherical head model (despite the fine tuning of its parameters) still involves a dramatic and systematic bias in the dipole estimation. To illustrate this point, the user has fitted a second source to the original unique-dipole solution corresponding to source 1. The new RV index dropped to 13 % and the second source shown equivalent magnitude in its moment than the original one (see Figure 4). This spurious source is here only to account for the model bias introduced by the sphere geometry approximation and its simplified conductivity parameters.

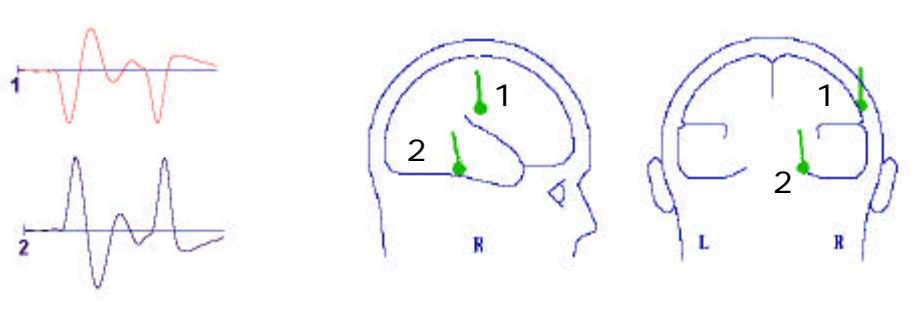


Figure 3 — Apparition of a phantom source when over-fitting the data to make the RV index decrease. Source 1 is very close to the original source location S1, while source 2 is a typical spurious or phantom source to account for the bias introduced by the simplified sphere model.

Processing dipole fit on real data sets implies working with this model bias, which is usually even greater in typical experiments than the one here as 3D localization of the electrodes, is still not a common practice. Further, the tuning of conductivity parameters is still not possible according to *in vivo* measurements.

In conclusion, as dipole fitting in a sphere model can give precious indications about the regions that are likely to be active, precise localization of the sources for anatomical registration should be processed with extreme care. This is especially the case when considering the minimum RV as the only quantitative guiding criterion. Important aspects like stability of the fitted source solution across time, and similarity of the scalp potential map with the original one have to play a central role in the source fitting strategy.

We now investigate another approach to the inverse problem for source estimation: the distributed source models.

3.2 METHODS BASED ON DISTRIBUTED SOURCE MODELS

3.2.1 BASICS OF SOURCE ESTIMATION METHODS USING DISTRIBUTED SOURCE MODELS

Estimating the source of EEG with distributed source models consists in first, distributing several dipole sources with fixed locations and orientations in the whole brain volume or on the cortical surface, then estimating their amplitudes from the data. For fixed positions and orientations, the relation between source moments and the data can be translated according to the following system:

$$\mathbf{M} = \mathbf{G}\mathbf{J} + \mathbf{b} \quad (2)$$

Where \mathbf{M} is a column vector gathering the measurements on N_M sensors at a given time instant; \mathbf{J} is a N column vector made of the corresponding dipole moments; \mathbf{G} is the $N_M \times N$ gain matrix which columns are the step responses (or so-called lead-fields, Hämäläinen *et al.* 1985) of every dipole source to the sensor array; \mathbf{b} is a perturbation vector.

This is a well-known formulation of numerous image reconstruction problems. Estimating the source amplitudes consists in solving this noisy linear system. Considering the physics of data formation in EEG (and MEG), source estimation is linked to Fredholm integral equations of the first kind and are consequently ill-posed (Tarantola 1987). For a given data set, there is no unicity of the possible source distributions. Further, after discretization to a limited number of sensors,

the corresponding \mathbf{G} operator is ill conditioned, thus exposing the solution to a non-continuous dependence on \mathbf{M} because of its high sensitivity to even small perturbations on data and the model (Varah 1973, Golub and Van Loan 1983). This problem belongs to the field of linear ill-posed inverse problems for image reconstruction or restoration. Methods for solving this problem, called inverse procedures, must take regularizing schemes into account to prevent the oscillatory behavior of the solutions in presence of noise (Demoment 1989).

Basically, regularization schemes in the field of electrical source imaging range from constrained Minimum-Norm or Semi-Norm inverse of the gain matrix (Rao and Mitra 1973, Hämäläinen *et al.* 1993, Pascual-Marqui *et al.* 1994), to minimization of regularized least-square cost functions such as:

$$\hat{\mathbf{J}} = \min_{\mathbf{J}} (U(\mathbf{J})), \quad (3)$$

where:

$$U(\mathbf{J}) = \|\mathbf{M} - \mathbf{GJ}\|_{\mathbf{R}}^2 + I L(\mathbf{J}). \quad (4)$$

\mathbf{R} is the variance-covariance matrix when a Gaussian noise component is assumed. I is a positive scalar that balances the respective contributions to $U(\mathbf{J})$ of the data attachment term and the prior term $L(\mathbf{J})$. The \mathbf{R} -norm is defined as follows:

$$\|\mathbf{M} - \mathbf{GJ}\|_{\mathbf{R}}^2 = (\mathbf{M} - \mathbf{GJ})^t \cdot \mathbf{R}^{-1} \cdot (\mathbf{M} - \mathbf{GJ}). \quad (5)$$

t stands for matrix transposition. As no significant noise correlation has been noticed during the silent time interval of the phantom EP's, we will assume $\mathbf{R} = \mathbf{s}^2 \cdot \mathbf{I}$, where \mathbf{I} is the \mathbf{R}^N identity operator and \mathbf{s}^2 is the noise variance.

The regularization operator $L(\cdot)$ can be either quadratic or not, depending on the nature of the priors that one wishes to take into account. For instance, in the field of neuroimaging, this operator has been chosen either as the identity operator – thus producing source estimates with Minimum Norm priors, which are similar to solutions from pseudo inversion of the gain matrix; gradient or weighted Laplacian operators (Pascual-Marqui *et al.* 1994), or non quadratic for non-linear source estimators. In this latter case, one can choose priors in terms of the L1 norm of the source amplitudes that can avoid some of the smoothing properties of the L2 norm priors (Matsuura and Okabe 1997).

Further, as extensively exposed in (Baillet and Garnero 1997) and (Phillips *et al.* 1997), the non-quadratic formulation of the priors may be linked to very numerous previous works in image restoration and reconstruction using Markov Random Fields models and associated stochastic algorithms (see the seminal work in Geman and Geman 1984). The methods used in (Baillet and Garnero 1997) and (Phillips *et al.* 1997) consist in introducing explicit *a priori*

information in order to recover sharp intensity gradients in the source image. Here, it is assumed that the source pattern is made of areas with smooth intensity changes that may be separated by jumps in source amplitude: this situation may occur for instance between adjacent but functionally *non-related* cortical areas possibly as the ones on both sides of a sulcus (see below). First, a system of neighborhood is designed between cortical areas. Then owing to Bayesian formalism, the priors are easily included in a maximum *a posteriori* (MAP) estimate of the source pattern. The Gibbs formulation of the a posteriori density of probability finally produces the $U(\mathbf{J})$ energy function in terms of the dipole magnitudes.

3.2.2 LOW RESOLUTION ELECTRICAL TOMOGRAPHY METHOD (LORETA)

Basics of LORETA

While using generic minimum-norm methods, it has been shown that deeper sources may not be recovered properly because more superficial dipoles with smaller magnitudes would be privileged for the same EEG/MEG data set. That is the reason why lead field normalization can be operated to give all the sources, close to the surface and deeper ones, the same opportunity of being nicely reconstructed with a minimum-norm technique. LORETA is a method that proceeds in this way. It has been first published in the formulation of a linear source estimate via the computation of a minimum semi-norm constrained inverse of the gain matrix (Pascual-Marqui *et al.* 1994). The implementation we have been using is based on a regularizing operator $L(.)$ as a weighted Laplacian operating on source amplitudes distributed in the whole inner head volume:

$$L(\mathbf{J}) = \|\Delta \mathbf{B} \mathbf{J}\|^2, \quad (6)$$

where Δ stands for the discrete Laplacian operator in terms of source intensities, and \mathbf{B} is a diagonal matrix for column normalization of \mathbf{G} .

The LORETA source estimate is obtained after zeroing the partial derivatives of the associated cost function in (4):

$$\hat{\mathbf{J}}_{\text{LOR}} = (\mathbf{G}'\mathbf{G} + I \Delta' \mathbf{B} \mathbf{B} \Delta)^{-1} \cdot \mathbf{G}' \mathbf{M} \quad (7)$$

LORETA Results

Spherical head model

Figure 5A shows the results of source estimation with LORETA with the spherical head model. The volume source distribution has been calculated at the 210ms-peak of the EEG data on a volumic grid of 2000 voxels in the inner head volume (3 sources per voxel). Table 3A gathers the position of the maximum of activity of the source solution, and the corresponding localization error.

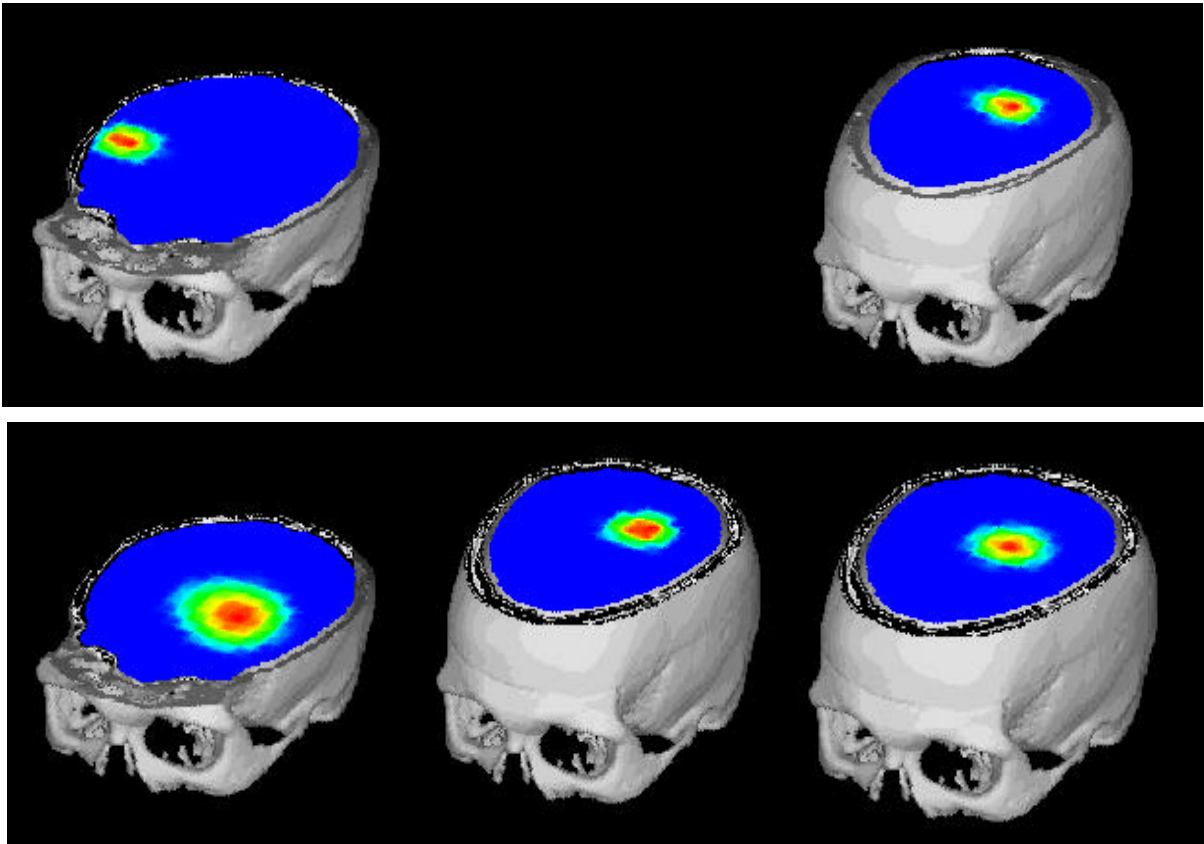


Figure 5A — Results from the LORETA inverse procedure using the spherical head model. These pictures correspond, from top left to bottom right to solution for activation of S1 to S6, respectively.

Source	Distance between the maximum LORETA source intensity and the true source locations (cm)
S1	4.0
S2	NC
S3	3.4
S4	1.9
S5	2.1
S6	2.0

Table 3A — Distance of LORETA maximum intensity spots to true source locations

LORETA seeks the solution with the smoothest intensity distribution owing to the Laplacian regularization priors. This kind of prior source model does not correspond to the

present focal shape of phantom sources. Thus, it will introduce a systematic source-model bias in the sense that focal sources will tend to be recovered in the form of a cloud of active sources which maximum is hopefully located at the true source position. Actually, the main issue of distributed source estimation methods is the *correct* choice for the regularization hyper-parameter value, λ . If λ is too large, too much credit is given to the smoothing priors and the estimated source shape tends to be uniform in intensity through the head volume (*i.e.* the source distribution for which the $L(\cdot)$ term is the smallest), thus corresponding to very poor data fit. On the other hand, if λ is too small, the inverse solution will tend to explain too well data (*i.e.* by correcting the head model simplifications by some localization bias, but also spurious sources, or even the *noise-related* perturbations on the original data set by *noise* sources). In this latter case, regularization is likely to be insufficient and the source image will tend to be corrupted by either spurious or *phantom* sources or, in the worst case, distributed oscillatory and sharp spatial changes in intensity from one point source to another.

An example of such behavior is given in Figure 6 where some over-fitting of data occurred. The original source is S1. While **A** is very close to the original source position, source **B** has no real existence. This is an artifact production of the algorithm to explain correctly the data. Unfortunately, the spherical head model and the weak prior hypothesis regarding the source distribution (namely in the whole head volume, and not on restricted areas), are not sufficient to remove most of the ambiguity of the source estimation. This source configuration, for the same data set, is very similar to the one found by BESA when small RV is achieved.

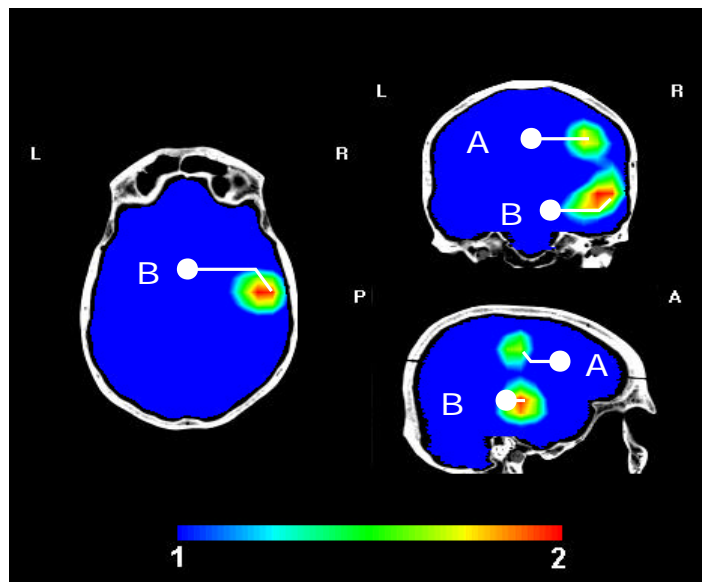
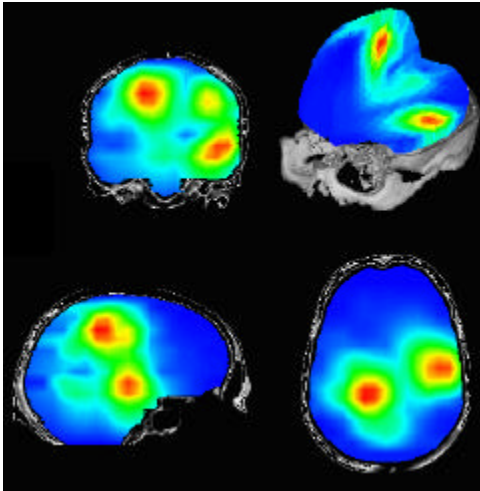


Figure 6 — LORETA source estimation for S1. This source model denotes over-fitting of the data very similar to the one obtained with BESA in Figure 4. **A** is the source cloud the closest to the original source (similar to source 1 in Figure 4), while **B** is a spurious source (that is similar to source 2 in Figure 4).

A complementary study is proposed here where 2 sources are simultaneously active. This phantom simulation is of interest to investigate the possible recovery of synchronous activity within some cortical areas. In that purpose, source S1 and S5 have been triggered with a simultaneous firing. They had the same kind of amplitude time courses, but with a 1/3 ratio between S1 and S3. Results are shown in Figure 5B and Table 3B,



Source	Distance between the maximum LORETA source intensity and the true source locations (cm)
S1	4.0
S5	2.1

Table 3B — Distance of LORETA maximum intensity spots to true source locations, synchronous firing.

D Figure 5B — LORETA source estimation for synchronous firing of sources S1 & S5

These results confirm the preceding findings for individual source firing. The localization errors are the same as before and the spurious activity associated to S1 is still present.

Conclusion

In the present study, the LORETA solutions to the inverse problem should be considered with care. Considering the position of the spot of maximum intensity in the reconstructed source image as the correct localization of the original focal source can be misleading for two main reasons: a) Some spurious source activity is likely to appear with sometimes larger intensity than the one at the true source location (see S1); b) The LORETA source model is not well suited for focal source estimation. Thus we think some grid refinement would be necessary for enhanced accuracy (at the expense of the computational cost). But further, the Variable Resolution Electrical Tomography (VARETA, (Valdes-Sosa *et al.* 1996)) focusing method inspired by the original algorithm seems to give promising results for focal source estimation. Unfortunately at this time, we are not able to show the results from VARETA for the estimation of the phantom sources.

We will now reduce the possible emergence of those spurious source components by restricting the source space dimension with the implementation of methods working on the cortical surface.

3.2.3 DISTRIBUTED SOURCE MODELS ON THE CORTICAL SURFACE

Introduction

To decrease the ambiguity on source localization in the whole head volume, a possible solution consists in restricting the search space in limited areas of the brain volume (e.g. the cortical surface). This approach has been first introduced in (Dale and Sereno, 1993) and is currently being used by several research groups (Baillet and Garnero 1997, Phillips *et al.* 1997) and the CURRY software by Philips (Neuroscan Inc.). A 3D segmentation of the brain surface allows the restricted distribution of the source space on the cortex. The dipolar sources are then constrained perpendicularly to the cortical surface. This latter constraint is a model of the organization of macro-columns assemblies of neurons in the gray matter which are very likely to be responsible for most of the EEG/MEG signals when fired with a sufficient degree of spatial and temporal coherence (Nunez 1981, Gloor 1985). This source space reduction, though introducing precious anatomical information and constraints, requires precise co-registration of MRI anatomical images with EEG and/or MEG.

We have adapted two inverse procedures that explicitly work on cortical source distributions. In the following subsections, we will investigate whether significant enhancements in localization accuracy can be achieved by these methods, even for simplified head models.

How to give this phantom a brain?

We have started from a tessellation of the cortical surface of a human brain, obtained after 3D segmentation of 128 MRI slices. The segmentation method we have used here operates the extraction of the white matter / gray matter interface (Mangin *et al.* 1995). The final surfacic mesh is made of 29,192 triangles corresponding to 14,596 vertices (see Figure 8).

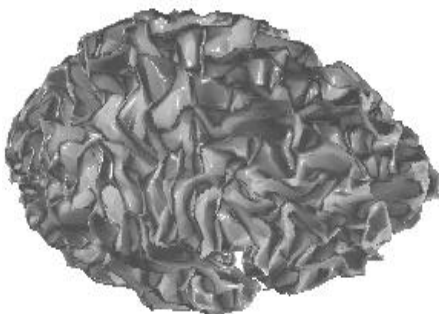


Figure 8 — The original cortical surface before it has been fitted to the phantom head.

After registration of the cortex mesh in the CTScan coordinate system, global linear transformations have been applied to scale the original brain volume so that it could fit the phantom head (Figure 9).

Finally, local linear transformations are applied in order that the original 6 source locations belong to the cortical surface. The orientations of the normals to the cortical surface are also locally adapted so that they correspond to the actual source orientations. Different views in Figure 10 show the final cortical surface with the original sources plotted as arrows. The source space is then defined over a set of 506 sources corresponding to some of the 14,596 original vertices. 6 sources are located and oriented according to the original current sources, while the other 500 are distributed according to uniform spatial sampling of the cortical surface.

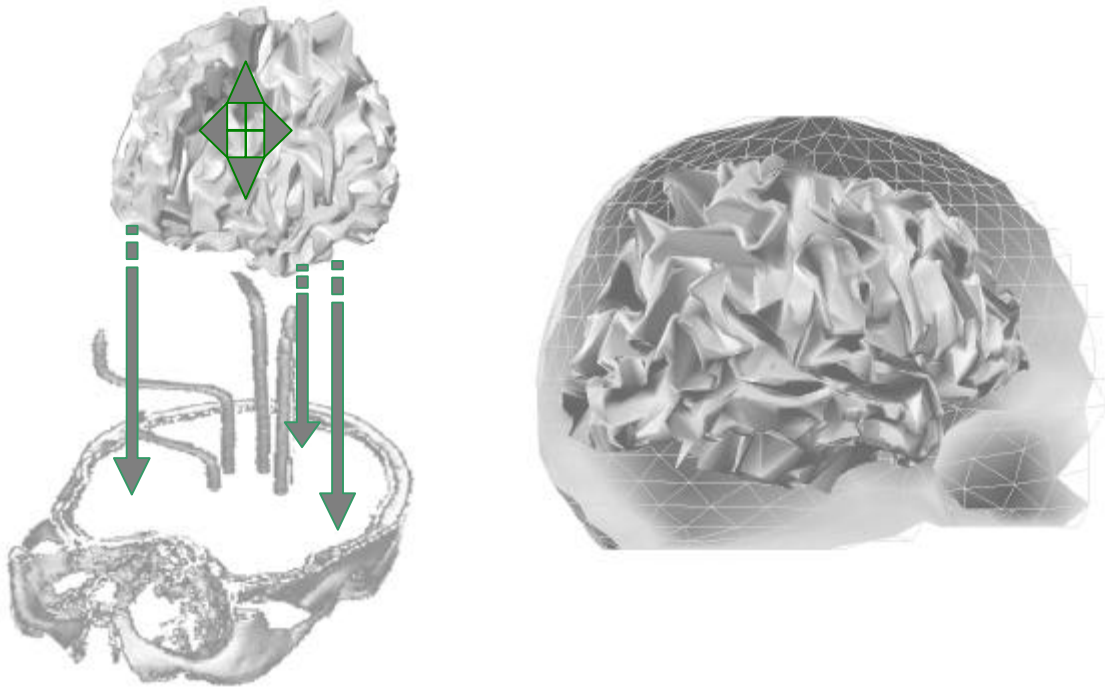


Figure 9—Global transformation of the original cortical surface, and scaling to the inner volume of the phantom head (left); a representation of the cortical surface fitted in the phantom head volume.

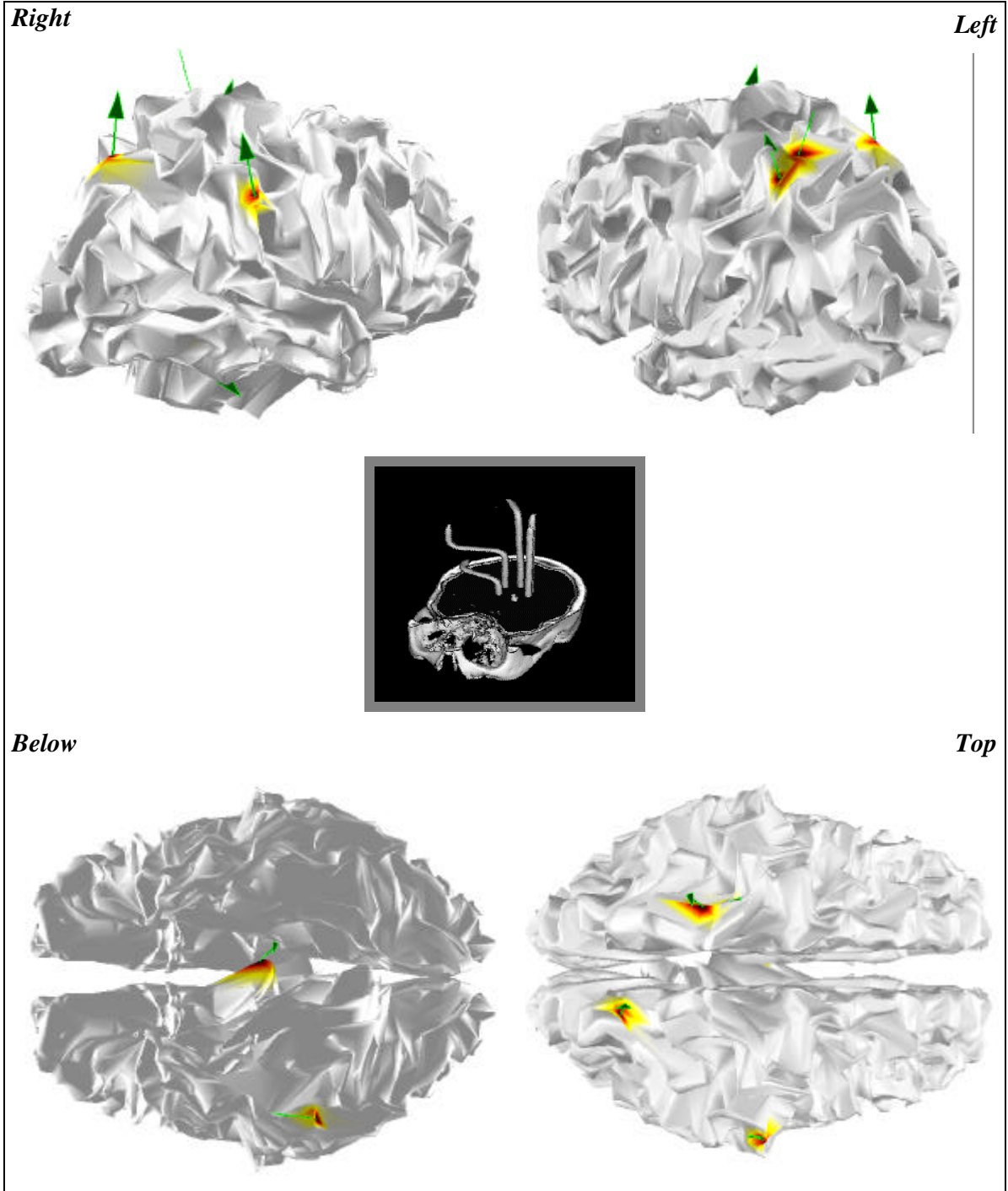


Figure 10 — Original source positions on the original CTScan (center) and their corresponding positions on the virtual phantom cortex. The arrows are pointing along the local normals to the cortical surface, which correspond to the actual source orientations. The intensity spots on the cortical surface at the bottom of each arrow represent a cortical map of the dipole amplitudes (here they have the same unit amplitude (arbitrary unit)).

Regularized Solutions with Minimum-Norm Priors

1.3.2.3.1.1 Method

Minimum-norm estimates (MNE) are based on a search for the solution with minimum power. This kind of prior is well suited to distributed source models where the activity is likely to extend over some areas of the cortical surface. Nevertheless, in the case of spatial sub-sampling of the cortical surface, like in the present case, it is very likely that such model will introduce a systematic bias in the reconstructed source pattern by over estimating the extension of the source intensity pattern.

Some implementations of MNE use constrained inverse of the gain matrix for MN solutions to the noisy linear system in (2) (Radhakrishna Rao and Mitra 1973, Golub and Van Loan 1983, Hämäläinen *et al.* 1993). The solution is calculated by application of a pseudo-inverse of the \mathbf{G} matrix to the noisy data vector. The main problem here is that the associated MNE are not regularized and suppose *i*) that no noise is present on data and *ii*) that \mathbf{G} is a well conditioned operator. While the first condition may be practically achieved on EP data with high SNR, the \mathbf{G} operator is always ill-conditioned when many sources in the distributed source model have close orientations and positions, and thus similar contributions to data. Another approach consists in adopting the formulation of a regularized inverse problem, by tuning the participation of the MN prior term $L(\mathbf{J}) = \|\mathbf{J}\|^2$ in the global cost function in (4) (Tikhonov and Arsenin, 1977).

We have chosen this latter implementation and thus the MNE of the source activity is given by:

$$\hat{\mathbf{J}}_{MNE} = (\mathbf{G}'\mathbf{G} + \mathbf{I}\mathbf{I}_N)^{-1} \cdot \mathbf{G}' \cdot \mathbf{M} \quad (8)$$

when $N_M > N$, or

$$\hat{\mathbf{J}}_{MNE} = \mathbf{G} \cdot (\mathbf{G}\mathbf{G}' + \mathbf{I}\mathbf{I}_{N_M})^{-1} \cdot \mathbf{M} \quad (9)$$

when $N > N_M$ (Tarantola 1987).

1.3.2.3.1.2 Results

MNE have been computed for the six sets of data where each current source has been individually fired.

Results are presented according to 4 criteria:

\mathcal{E}_{max} : the distance in cm between the location of the maximum in intensity of the estimated activity ($\mathbf{J}_{max} = \max_{k \in [1, 2, \dots, N]} \left(\left| \hat{\mathbf{J}}(k) \right| \right)$) and the actual source position. In MNE, \mathbf{J}_{max} is usually considered as an index of the true activity location, though this could lead to significative errors (see above).

E_{max} : the relative energy contained in \mathbf{J}_{max} with regards to global energy in \mathbf{J} .

$$E_{max} = 100 \times \frac{\mathbf{J}_{max}}{\|\hat{\mathbf{J}}\|} \quad (\%) \quad (10)$$

\mathcal{E}_G : the distance between the actual source location and the position of \mathbf{J}_G , the gravity center of the source estimate. This criterion gives quantification of the visual aspect of the source pattern, while taking all the source intensities into account. \mathcal{E}_G is defined as follows:

If $l(k)$ is the location of the k^{th} source with intensity $\hat{\mathbf{J}}(k)$ and l_o the original source location with intensity J_o , then:

$$\mathbf{e}_G = \left| \frac{\sum_{k=1}^N \hat{\mathbf{J}}(k) \cdot l(k)}{\sum_{k=1}^N \hat{\mathbf{J}}(k)} - l_o \right| \quad (mm) \quad (11)$$

$E_{spurious}$ is the relative energy contained in spurious or phantom sources with regards to the original source energy.

These criteria will be used in the next subsections for the other inverse procedures.

Results for MNE are gathered in Table 4.

	<i>FEManiso</i>				<i>Sphere</i>				
	\mathcal{E}_{max} (cm)	E_{max}	\mathcal{E}_G (cm)	$E_{spurious}$	\mathcal{E}_{max} (cm)	E_{max}	\mathcal{E}_G (cm)	$E_{spurious}$	
S1	0.00	54%	2.68	46%	S1	0.00	48%	2.79	52%
S2	2.33	3%	3.82	98%	S2	1.99	10%	4.53	98%
S3	2.38	10%	4.26	98%	S3	1.01	12%	4.43	96%
S4	8.29	5%	4.01	100%	S4	8.42	9%	4.83	100%
S5	0.94	20%	2.92	93%	S5	1.32	24%	3.19	83%
S6	2.05	13%	2.69	94%	S6	2.05	15%	2.99	93%
<>	2.66	18%	3.40	86%	<>	2.48	20%	3.79	87%

Table 4 — Summary of MNE accuracy with both the FEManiso and the Sphere models.

The notation $\langle \rangle$ indicates the average value of the current column.

It is striking to see that MNE produces very poor estimation of the true source locations with *both* the realistic *FEManiso* and the simplified *Sphere* models. The introduction of the real head geometry and the related conductivity properties brings no significant enhancement to the source estimation accuracy. We can notice high rates of spurious activity for which the center of gravity is more than 3cm away from the true activity spot on the average. Even the location of the spot of maximum intensity is a very bad indicator of the actual source location (especially for deeper source S4).

We illustrate these results further in Figure 11 and 12 where the distribution of estimated activity for sources S1 and S6 respectively are interpolated on the cortical surface. While results are satisfactory for S1, the picture for S6 gives an indication of the difficulty to interpret phantom sources with large intensity that may appear at some distance of the true source location.

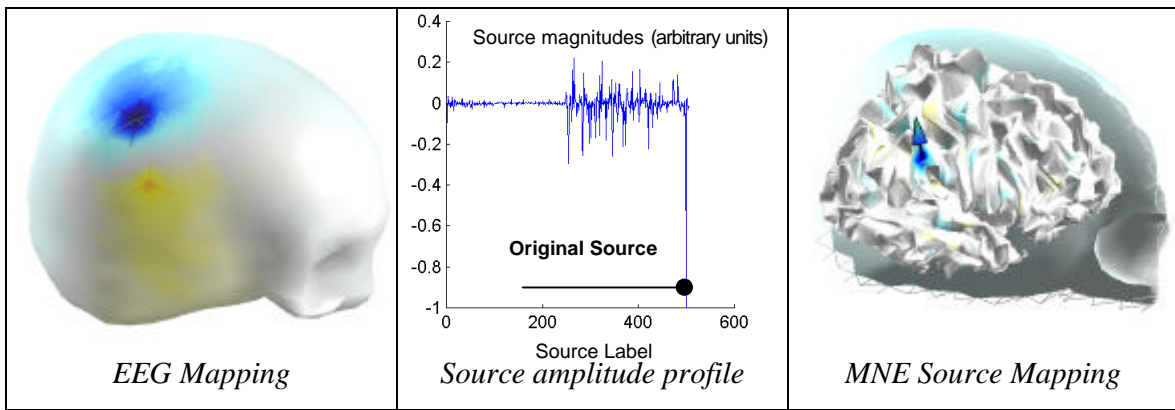


Figure 11 — Source S1: Scalp potentials mapping and MNE estimate illustration. Please note the numerous spurious activity spots. Nevertheless, the main site of activity (arrow) is correctly located.

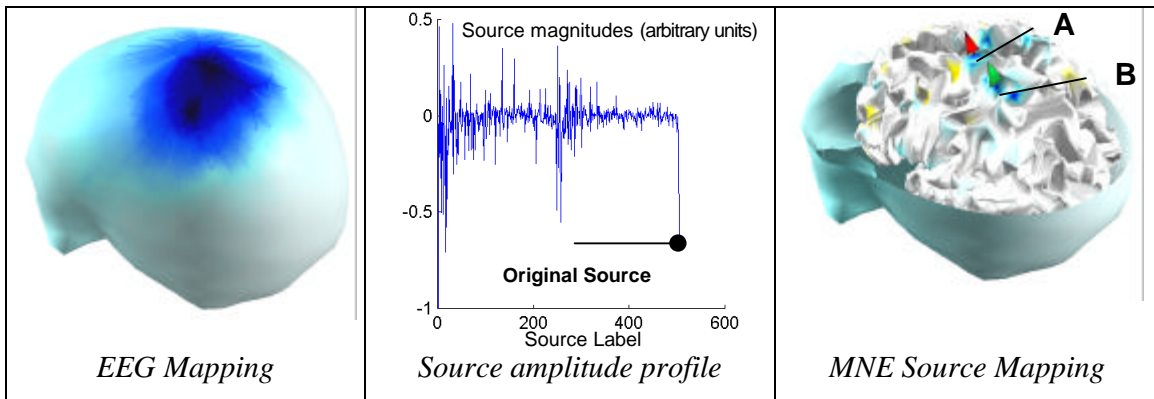


Figure 12 — Source S6 : Scalp potentials mapping and MNE estimate illustration. Here the source with maximum intensity (A) is not properly located at the true focus location (B).

Thus, MNE even with realistic head models gives poor estimates of focal activity on the cortex. This is mainly due to the bad affinity of the prior model with the spatial sampling of the source space. Here about 500 sources are uniformly distributed over the whole cortical surface. At this scale of description of the source distribution, it is likely that some focal spots of activity may appear, and the minimum-norm (*i.e.* minimum power) source model is not well suited to this kind of source activation pattern.

We will now investigate the merits of a method that is particularly well suited to the estimation of focal activity patterns.

MNE with FOCUSS

1.3.2.3.1.3 Method

FOCUSS is a recursive procedure of weighted minimum-norm estimations of the source pattern (Gorodnitsky *et al.* 1995). This method has been developed to give some focal resolution – close to the one attributed to spatio-temporal dipole models - to linear estimators based on distributed source models. The main idea consists in recursively produce MNE with iterative weighting of the columns of the gain matrix \mathbf{G} , based on the amplitudes of the sources at the previous iteration.

Basically the source estimation at iteration i of the source amplitudes is written:

$$\hat{\mathbf{J}}_{FOCUSS|i} = \mathbf{W}_i (\mathbf{G}\mathbf{W}_i)^+ \mathbf{M}, \quad (12)$$

where $(\mathbf{A})^+$ denotes the Moore-Penrose pseudo-inverse of matrix \mathbf{A} ; and \mathbf{W}_i is a diagonal matrix defined as follows:

$$\mathbf{W}_i = \mathbf{w}_i \cdot \mathbf{W}_{i-1} \cdot \text{diag}\left(\left|\hat{\mathbf{J}}_{i-1}\right|\right) \quad (13)$$

\mathbf{w}_i is a diagonal matrix for deeper source compensation:

$$\mathbf{w}_i = \text{diag}\left(\frac{1}{\|\mathbf{G}(:,j)\|}\right), j \in [1,2,\dots,N] \quad (14)$$

where $\mathbf{G}(:,j)$ is the j^{th} column of the gain matrix (*i.e.* the lead-field associated to source j).

Our implementation uses MN as an initial solution and some regularization of the source estimation with quadratic priors (as recommended in (Gorodnitsky *et al.* 1995) in presence of

noisy data) instead of the Moore-Penrose pseudo-inverse. The regularized formulation operates on the same cost function as in (4) after the following transformation of variables has been done:

$$\begin{cases} \hat{\mathbf{G}} = \mathbf{G} \cdot \mathbf{W}_i \\ \hat{\mathbf{J}} = \mathbf{W}_i^{-1} \cdot \mathbf{J} \end{cases} \quad (15)$$

1.3.2.3.1.4 Results

The results for FOCUSS working on the *FEManiso* model are gathered in Table 5.

<i>FEManiso</i>				
	ϵ_{\max} (cm)	E_{\max}	ϵ_G (cm)	E_{spurious}
S1	0.00	85 %	0.90	15 %
S2	0.98	100 %	0.93	100 %
S3	2.04	88 %	1.96	100 %
S4	8.74	13 %	5.15	100 %
S5	0.00	100 %	0.00	0 %
S6	0.00	100 %	0.00	0 %
<>	1.96 / 0.60	81 / 95 %	1.5 / 0.77	53/43 %

Table 5 — Summary of localization accuracy of FOCUSS with the *FEManiso* head model. Here, the average values are computed over the 6 sources and the 5 sources without considering *S4* respectively.

First, localization accuracy is impressively improved, in comparison to MNE, owing to iterative focusing. Sources S1, S5 and S6 are perfectly estimated. S2 is located with a *1cm* bias and with little spurious activity. S3 position is not properly estimated. This could be due to its very close location to the skull, hence: *i*) numerical errors in the FEM solution to the forward solution are very likely (Marin *et al.* 1998), *ii*) the SNR is low on a majority of electrodes, as there is few potential scattering of the scalp potentials for this kind of superficial sources. S4 location is not properly estimated either: here also, the SNR on all electrodes is much weaker than for the other sources with a very low signal level on the whole sensor array. We give in Table 5 the average values of the quantification criteria for both every source and for the whole source set deprived of S4. Then, sub centimeter precision is achieved on the average, but sources like S2 and S3 are still not correctly located.

Results with the *Sphere* model are now presented in Table 6.

<i>Sphere</i>				
	ϵ_{\max} (cm)	E_{\max}	ϵ_G (cm)	E_{spurious}
S1	0.00	85 %	0.90	15 %
S2	0.98	100 %	0.99	100 %
S3	1.09	60 %	1.42	100 %
S4	4.68	93 %	1.61	100 %
S5	0.00	100 %	0.00	0 %
S6	0.00	98 %	0.41	2 %
<>	0.63 / 0.41	89 / 89 %	0.9 / 0.76	52/43 %

Table 6 — Summary of localization accuracy of FOCUSS with the *Sphere* head model. The average values are computed over the 6 sources and the 5 sources without S4 respectively.

These results are very similar to the ones obtained with the *FEManiso* head model. We can see that errors on S3 are smaller than with *FEManiso*. Actually, the errors are partly corrected by the analytical solution to the forward model. The location bias for this source is then similar to the one obtained for S2. Some very little spurious activity is now visible on S6 (see Figure 13). But the main issue regards the location error on S4, which is still notably high. This indicates that the localization of deeper sources like the one in the brain stem or basal ganglia can not be properly estimated with EEG.

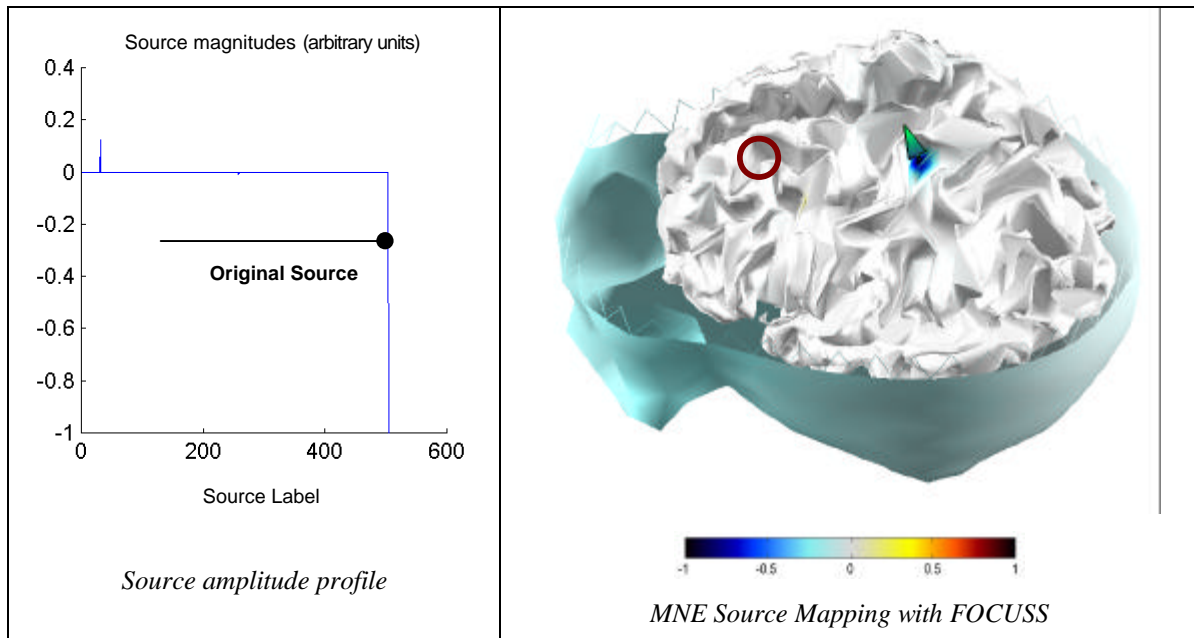


Figure 13 — Estimation of S6 with FOCUSS. The original source is well recovered with only some very little spurious activity in the frontal area (marked with the circle).

One possible issue of focusing estimation methods is that they could fail in recovering simultaneous activation of the underlying sources. To investigate this point, we have selected the EEG recording where S1 and S5 were fired simultaneously. S1 having amplitude that was one third of S5's.

The FOCUSS estimation has been computed on 41 time samples of the related EP.

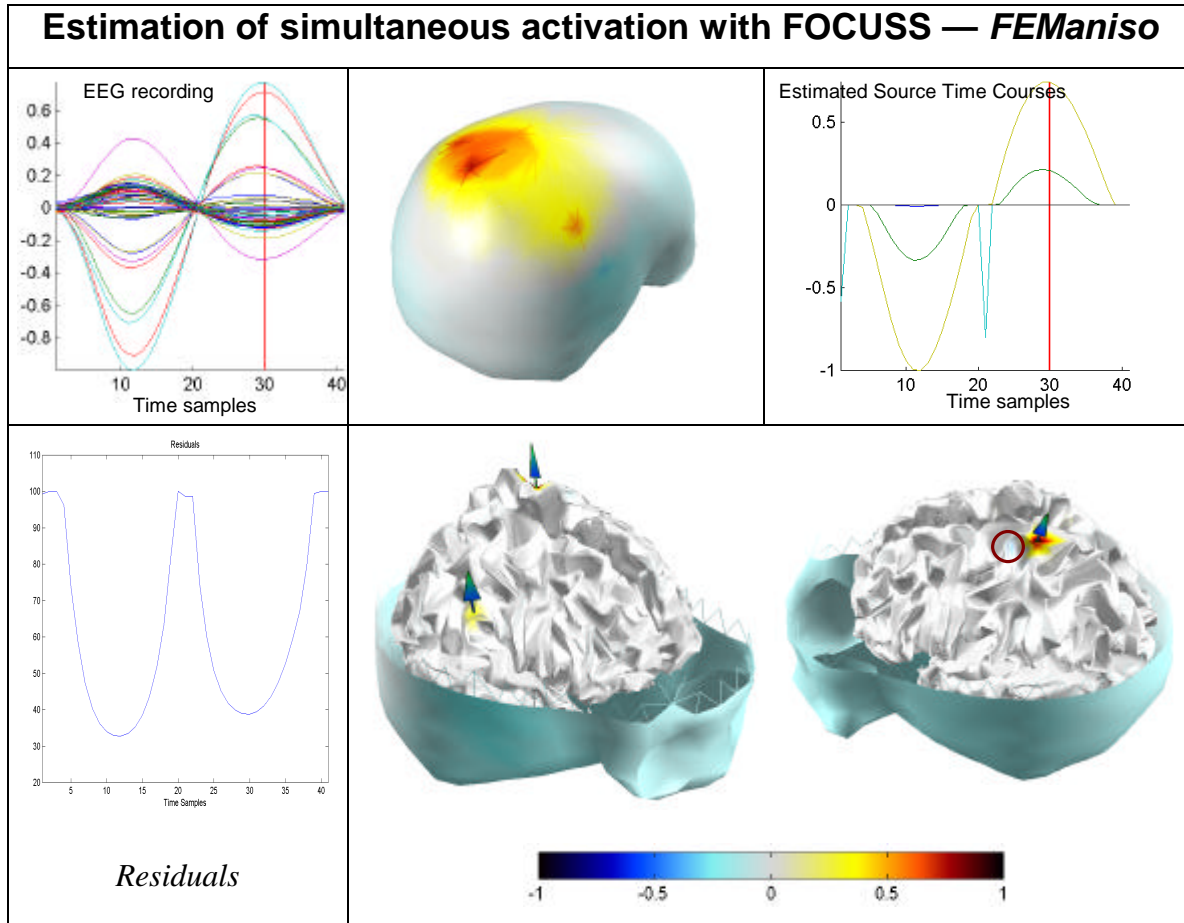


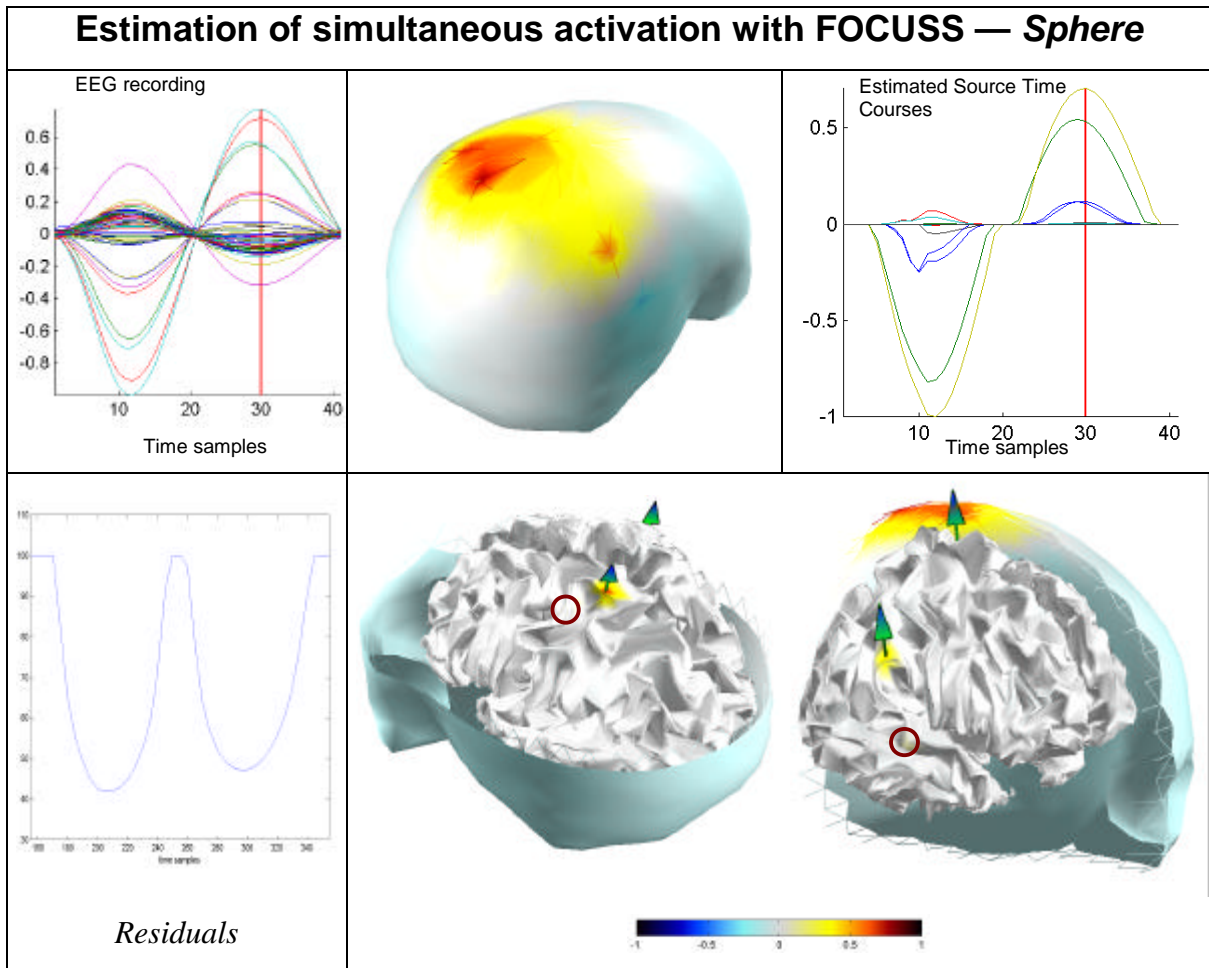
Figure 14 — Estimation of synchronous activity with FOCUSS. Hardly is seen very little spurious activity (marked with the circle). The respective time courses of the active dipoles are quantitatively well recovered.

Figure 14 gathers the original data and the FOCUSS results for the *FEManiso* head model. The “residuals “ plot shows the relative ratio of data that remains unexplained by the current source estimation.

It appears that the original source locations are still very nicely estimated, with little spurious activity on some other sources. Further, the magnitude ratio of 1/3 between S1 and S5 is also correctly recovered. Nevertheless, some instability in the source estimate appears at the data zero-crossing time instants (around sample n°21). Here, the residuals in the data that remain unexplained by the source estimate is very high and comparable to what happens at the borders of the EEG epoch, where there is little signal power.

We have pursued this investigation by the use of the Sphere model to check the robustness of synchronous activity estimation with simplification of the head model.

Results are displayed and summarized in the next figure (Figure 15).



*Figure 15 — Estimation of synchronous activity with FOCUSS, Sphere model.
Hardly is it seen very little spurious activity (marked with the circle).
The respective time courses of the active dipoles are quantitatively well recovered.*

This time, though the basic time course of activity of sources S1 and S5 is still properly recovered, the quantitative 1/3 ratio in amplitudes is not well estimated any more. Further more spurious source activities appear in some regions that may be quite far from the actual source positions (see circles in Figure 15). Because of this spurious activity, the question raises that it may be difficult in practice to draw definitive conclusions regarding the reality of some of the sources in the final source image. How is it possible to define some threshold to classify the true sources from the others (especially when the residual rates are high, like in this latter case (> 40%), which means that the present sources are essential to the explanation of the data)?

1.3.2.3.1.5 Conclusion

When a single focal source is to be estimated, the FOCUSS algorithm succeeds in properly assessing most of the original locations, except for deeper sources (like S4) or closer ones (like S3). For this latter, it is likely that both numerical errors in the FEM calculation (for the *FEManiso* model) and the little number of electrodes with significant SNR levels (with both the *FEManiso* and *Sphere* models) are responsible for this poor accuracy. SNR level for deeper sources like S4 is too low for proper source localization. There is also a systematic bias in the localization of S2 (which is rather deep and tangential).

In that very particular case, there is no justification for the use of a complex model such as *FEManiso* in comparison to the performance achieved with the *Sphere* model. Finally, simultaneous activation of two sources that were previously perfectly recovered independently with both the *Sphere* and the *FEManiso* model is better estimated with the more realistic head model. Actually, the use of spherical geometry facilitates the apparition of spurious activity, though with smaller magnitudes than the true sources and may make the final source image quite arduous to explain.

In the last subsection, we operate some refinement in the source prior model by the design of a non-quadratic cost function in terms of source intensity. We will check whether a more sophisticated source model would allow more accurate and robust source estimation, for every head models.

The ST-MAP inverse procedure.

1.3.2.3.1.6 Basics of ST-MAP for the estimation of focal sources

As mentioned above, ST-MAP is an inversion procedure based on a non-quadratic priors in terms of dipole intensity (Baillet and Garnero 1997). It is related to many previous works in image restoration (Blake and Zisserman 1987, Geman and Mac Clure 1987, Geman and Reynolds 1992) and their extension to tomography image reconstruction (Gindi *et al.* 1993, Charbonnier *et al.* 1996).

ST-MAP has been primarily designed for the recovery of homogeneous intensity patches in the source image, that may be separated by anatomical and functional edges. Though MNE, or more generally, linear estimators produce smooth intensity images, the introduction of non-

quadratic priors make the source estimator becomes non-linear and appropriate to the detection of intensity jumps.

Basically, after a system of neighborhood has been designed on the cortical surface, the prior term in (4) may be written as the sum of locally defined potentials:

$$L(\mathbf{J}) = \sum_{n=1}^{N_v} \Phi_v(\nabla \mathbf{J}_v) \quad (16)$$

We denote ∇ as the gradient operator over the dipole amplitudes ($\nabla \in \mathfrak{R}_{N_v, N}$, where $N_v = N \times N_n$, and N_n is the number of neighbors for each source j), $\nabla \mathbf{J}_v$ as the v^{th} element of the spatial gradient vector. The Φ -functions are defined in terms of normalized intensity gradients $u = \nabla \mathbf{J}_v$ as follows:

$$\Phi_v(u) = \frac{u^2}{1 + \left(\frac{u}{K_v}\right)^2} \quad (17)$$

where K_v plays the role of a local detection threshold of intensity jumps in the source pattern. Actually for small gradients the local cost is quadratic, thus producing areas with smooth spatial changes in intensity, whereas for higher gradients, the associated cost is finite - $\Phi_v(u) \approx K_v$ - thus allowing the preservation of discontinuities in the source image despite the needs for regularization. The threshold values where intensity jumps are not likely are higher than where there may be some functional edges on the cortical surface.

As there is no possible definition of functional edges on the phantom cortical surface, we will only rely on anatomical variations of the *virtual cortex* inside the neighborhood system of a given dipole for the definition of the detection thresholds.

1.3.2.3.1.7 Design of the detection thresholds according to the anatomy of the cortex.

For every vertex of the cortical mesh, the 4 closest vertices in terms of the Euclidean distance are designated as the neighbors of the current source (*i.e.* $N_n = 4$). Then, for every source of the current neighborhood, the corresponding weighting coefficient K_v is computed according to:

$$K_v = \mathbf{a}_v \times \mathbf{b}_v \quad (18)$$

where \mathbf{a}_v depends on the distance between the source and the current neighbor; and \mathbf{b}_v is a coefficient indexed on the discrepancy regarding the orientations of the two sources considered here. Both of these scalars are scaled in the interval [0,1]. It is essential to index the detection thresholds on the source orientation as close sources may be located on opposite walls of the same sulcus. As a consequence, they may be considered as functionally non-dependent (thus there is an

important debate in that field (Roland *et al.* 1997, Régis *et al.*1995)) or at least as interacting contributors to the data. It means that these sources possess some very similar absolute lead-fields that make them difficult to discriminate in the inverse procedure. If some prior information introduces explicitly the possibility of intensity jumps between these two sources, it will facilitate the discrimination in the estimation of their respective amplitudes (see Figure 16).

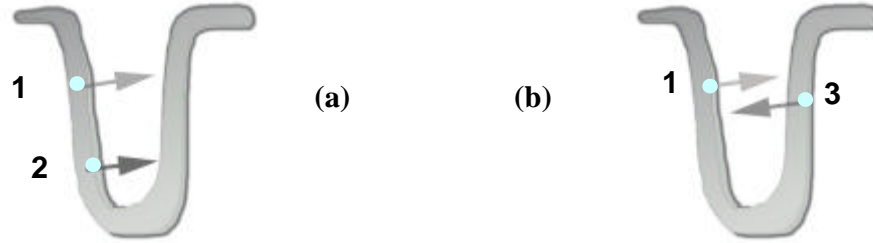


Figure 16 — An illustration of how to adapt the weighting coefficients of the neighborhood system. (right) Sources 1 and 2 are on the same sulcus wall and have similar orientations; (left) Sources 1 and 3 are at the same distance than previously 1 and 2, but with opposite orientations as they are on opposite walls of the same sulcus.

The weighting coefficients \mathbf{b}_v should be scaled in such a manner that for equivalent \mathbf{a}_v values (case (a) and (b) in Figure 7), the apparition of intensity discontinuities between sources 1 and 3 in case (b), should be favored. In our case, we have chosen the following definitions for respectively \mathbf{a}_v and \mathbf{b}_v .

$$\left\{ \begin{array}{l} \mathbf{a}_v = 1 - \frac{d_{kv}}{\max_{j \in [1, 2, \dots, N_n]} (d_{kj})} \\ \mathbf{b}_v = \frac{(1 + \vec{n}_k \cdot \vec{n}_v)}{2} \end{array} \right. \quad (19)$$

where d_{kv} is the distance between source k and its neighbor, labeled v . \vec{n}_k (res. \vec{n}_v) is the unit orientation vector that indicates the orientation of dipole k (res. its neighbor v). Note that when source k and v have similar orientations, the related K_v coefficient varies gently with the distance between them, while when they are facing each other, K_v is close to 0 because $\vec{n}_k \cdot \vec{n}_v \rightarrow -1$.

Once these weighted neighborhood system has been designed on the whole cortical surface, we propose here a focusing implementation of the original ST-MAP algorithm that has been firstly designed for the recovery of source intensity patches (Baillet and Garnero 1997).

1.3.2.3.1.8ST-MAP with iterative focusing

Without going into too much details with the practical implementation of the ST-MAP estimation, we now propose a modified version of the algorithm that is dedicated to the recovery of focal sources when the spatial sampling of the cortical surface is sparse. The main idea here consists in reducing the source space dimension by iterative focusing on the regions that have been previously estimated with *significant* activity.

The original ST-MAP estimator is an iterative procedure of successive linear estimations of the source pattern in the following way:

At iteration step i :

$$\hat{\mathbf{J}}_i = \Theta(\mathbf{G}, L(\hat{\mathbf{J}}_{i-1})) \cdot \mathbf{M} \quad (20)$$

where $\Theta(\mathbf{G}, L(\hat{\mathbf{J}}_{i-1}))$ is a $N \times N_M$ matrix depending on the original gain matrix \mathbf{G} and priors computed from the previous source estimate $\hat{\mathbf{J}}_{i-1}$ according to (16). This iterative scheme is repeated until convergence.

The modified ST-MAP consists in operating recursive refinement by reduction of the column dimension of \mathbf{G} along the iterations i . We now note \mathbf{G}_i the column-reduced version of \mathbf{G} at iteration step i , with a selection of $N_i \leq N$ sources. This implementation allows the reduction of the source space to up to few sources while the others are set to null amplitude, which is very consistent with focal estimation purposes. At iteration step i , the N_i sources are selected according to the following consideration:

Sources with either large amplitudes and/or large contribution to data should be candidates for the next iteration step. Thus, an energy criterion is designed with dependence on both source intensities and contribution to data.

$$E = 2.E_c + E_a \quad (21)$$

where E_c is the term quantifying the contribution of every dipole source to the data, and E_a is an index of dipole relative amplitudes. Factor 2 indicates that a preference is afforded to sources with more contribution to data than large amplitude, which is a regularizing setting. Energy associated to dipole j is written $E(j)$.

E_c gathers the dot products between \mathbf{M} and every potential $\mathbf{G}(:, j) \cdot \hat{\mathbf{J}}_i(j)$ computed from the current source model, after scaling to 1 in absolute value.

E_a is defined according to:

$$E_a(j) = \frac{\left(\frac{\bar{\mathbf{J}}_i(j)}{0.1}\right)^2}{1 + \left(\frac{\bar{\mathbf{J}}_i(j)}{0.1}\right)^2} \quad (22)$$

where $\bar{\mathbf{J}}_i(j) = \frac{|\hat{\mathbf{J}}_i(j)|}{\max_j(|\hat{\mathbf{J}}_i(j)|)}$. $E_a(j)$ has values on the order of 1 for source magnitudes larger than 0.1, which is very favorable to the elimination of most of the sources with little amplitudes if they weakly contribute to data (see Figure 17), which is often characteristic of large interacting sources that could appear during the early iterations of the algorithm.

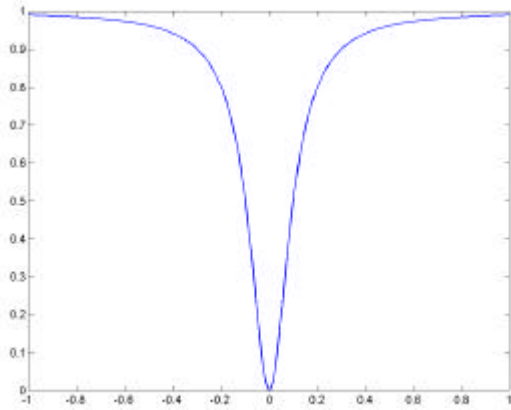


Figure 17 — Plot of the $E_a(u)$ energy function

$$E_a(u) = \frac{\left(\frac{u}{0.1}\right)^2}{1 + \left(\frac{u}{0.1}\right)^2}$$

Then, sources with energy larger than:

$$\mathbf{c}_i = \langle E \rangle + \frac{i}{\log(N)} \mathbf{s}(E) \quad (23)$$

are selected for the next iteration. $\langle E \rangle$ (res. $\mathbf{s}(E)$) stands for the average (res. standard deviation) of E . The selection threshold is thus dependent on i , indicating that many sources are selected during the early iterations. Note that selectivity operates as the recursion goes.

The corresponding linear system of reduced dimension is now:

$$\hat{\mathbf{J}}_i = \Theta(\mathbf{G}_i, L(\hat{\mathbf{J}}_{i-1})) \cdot \mathbf{M}. \quad (24)$$

This procedure has been evaluated on various numerical simulations and has produced satisfactory results, with the same head models and cortical surface than the ones used for the processing of recorded data.

In addition to the spatial focusing technique, we have used the temporal regularization prior described in (Baillet and Garnero 1997). It has been shown that this prior was essential for a better estimation of the dipole time courses on a time window of interest. This prior enforces continuity for the source time courses for the given time sampling cadence, which is consistent with the underlying physiological processes.

Briefly, the supplementary prior is a quadratic constraint of minimal projection of the source estimate at time t onto the perpendicular hyperplan defined by the previous source estimate $\hat{\mathbf{J}}_{t-1}$. Finally, the associated linear system is written:

$$\hat{\mathbf{J}}_i = \Theta(\mathbf{G}_i, L(\hat{\mathbf{J}}_{i-1}), \hat{\mathbf{J}}_{i-1}) \cdot \mathbf{M}. \quad (25)$$

1.3.2.3.1.9 Results

We now show the results obtained with the modified ST-MAP method for focal source estimation. This presentation is organized the same way as the previous ones but we will consider extensively all the available head models for single source estimation. Then, we will discuss the performance obtained on synchronous source firing.

Table 7 shows the results for single source estimation with the FEM and BEM models with realistic geometry.

<i>FEManiso</i>					<i>FEManiso_TR</i>				
	ϵ_{\max} (cm)	E_{\max} (%)	ϵ_G (cm)	E_{spurious} (%)		ϵ_{\max} (cm)	E_{\max} (%)	ϵ_G (cm)	E_{spurious} (%)
1	0.00	100	0.00	0	1	0.00	100	0.00	0
2	0.00	100	0.00	0	2	0.36	100	0.36	100
3	0.00	100	0.00	0	3	0.00	100	0.00	0
4	1.49	100	1.49	100	4	4.49	100	4.49	100
5	0.00	100	0.00	0	5	0.00	100	0.00	0
6	0.00	100	0.00	0	6	0.00	88	0.93	12
<>	0.25/0.00	100	0.25/0.00	20 / 0	<>	0.75/0.07	98	0.96/0.26	35 / 22

(a)

(b)

<i>FEMiso</i>					<i>BEM</i>				
	ϵ_{\max} (cm)	E_{\max} (%)	ϵ_G (cm)	E_{spurious} (%)		ϵ_{\max} (cm)	E_{\max} (%)	ϵ_G (cm)	E_{spurious} (%)
1	0.00	100	0.00	0	1	0.00	82	0.94	18
2	0.36	100	0.36	100	2	0.36	100	0.36	100
3	0.00	100	0.00	0	3	0.00	100	0.00	0
4	5.31	100	5.31	100	4	4.49	100	4.49	100
5	0.00	100	0.00	0	5	0.00	100	0.00	0
6	0.00	100	0.00	0	6	0.00	100	0.00	0
$\langle \rangle$	0.95/0.07	100	0.25/0.00	33 / 20	$\langle \rangle$	0.8/0.07	97	0.97/0.26	36 / 24

(c) (d)

Table 7 — ST-MAP results for head models with realistic geometry

The ST-MAP method allows the correct recovery of almost every dipole with FEManiso, except for the deeper S4 that is misallocated with an error of about 1.5cm. S2 and S3 are now perfectly recovered. Using simplified realistic models, the localization accuracy is very comparable from one model to the other. A little localization bias appears again on source S2 but remains acceptable ($< 4\text{mm}$), and smaller than the one obtained with FOCUSS (9.6mm). Very little spurious activity appears with BEM in the estimate related to source S1 (82% of the source power is concentrated in the source with maximum intensity). Thus a more sophisticated prior dipole model allows the recovery of the most superficial sources despite simplification in the conductivity parameters of the model.

In the next table are gathered the localization results regarding the use of the *Sphere* model (Table 8).

<i>Sphere</i>				
	\mathcal{E}_{\max} (cm)	E_{\max} (%)	\mathcal{E}_G (cm)	E_{spurious} (%)
1	0.00	100	0.00	0
2	0.00	100	0.00	0
3	0.00	100	0.00	0
4	1.49	100	1.49	100
5	0.00	100	0.00	0
6	0.00	100	0.00	0
<>	0.25/0.00	100	0.25/0.00	20 / 0

Table 8 — Results from the ST-MAP method, using the Sphere model.

Now it is interesting to note that the performances of ST-MAP using the sphere model are equivalent to the ones obtained with the most realistic model *FEManiso*. These results are even better than when using the other models with realistic geometry. This may be due to the fact that the loss of information regarding geometry and the fine conductivity parameters may be compensated by the resolution of the forward problem with the analytical formulation, thus producing better conditioned gain matrices \mathbf{G} . Finally, the associated linear system is less sensitive to perturbations on data and the head model than the ones associated to numerical resolution of the forward problem.

We think these are some encouraging results that come to confirm the good behavior of the localization ability of the spherical head models for the estimation of focal sources (see for instance Ebersole 1994, Leahy *et al.* 1998, and below).

We will terminate this study by the processing of the data set generated by synchronous firing of current sources S1 and S5. The question remains the same: is the spherical model doing as well as the FEM approach with anisotropy parameters? We now drop here the comparison with other models with realistic geometry.

Figure 18 gathers the results obtained with the *FEManiso* head model. The original synchronous sources are properly recovered with ST-MAP. The average residuals of unexplained data represent about 20% of the original data power. The source time courses are correctly estimated with little spurious activity at the zero crossing of potentials.

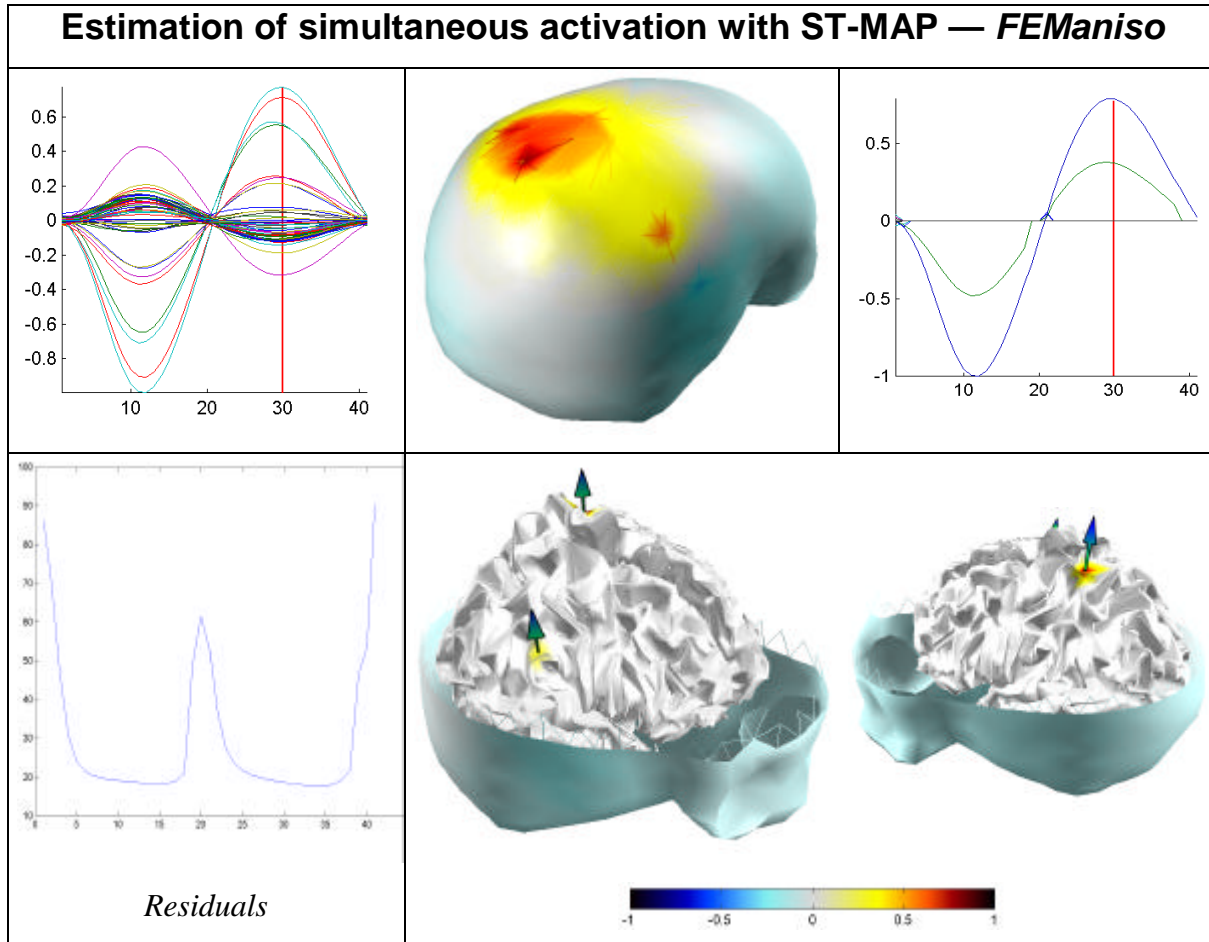


Figure 18 — The results from ST-MAP estimation of synchronous activity with the *FEManiso* model.

Finally Figure 19 shows the processing of the same data set but this time with the *Sphere* head model. Here again, there is no significant spurious activity in the source estimate, and the true active sources are correctly recovered, even at zero crossing potentials. Quantitatively, the 1/3 ratio on source magnitudes is no longer properly recovered, and the residuals raises to about 40% along the EP waves (see discussion below). Despite such high value of residual power, the reconstructed potential maps look really similar to the original ones. The signal on sensors with high SNR is well explained by the source model while there is more discrepancy on the other leads but with limited effect of the potential scalp map.

Relatively high values of residuals should not be considered as pathological as long as the source model explains correctly the topography of the potentials on the head, with sufficient persistence along a time window of interest.

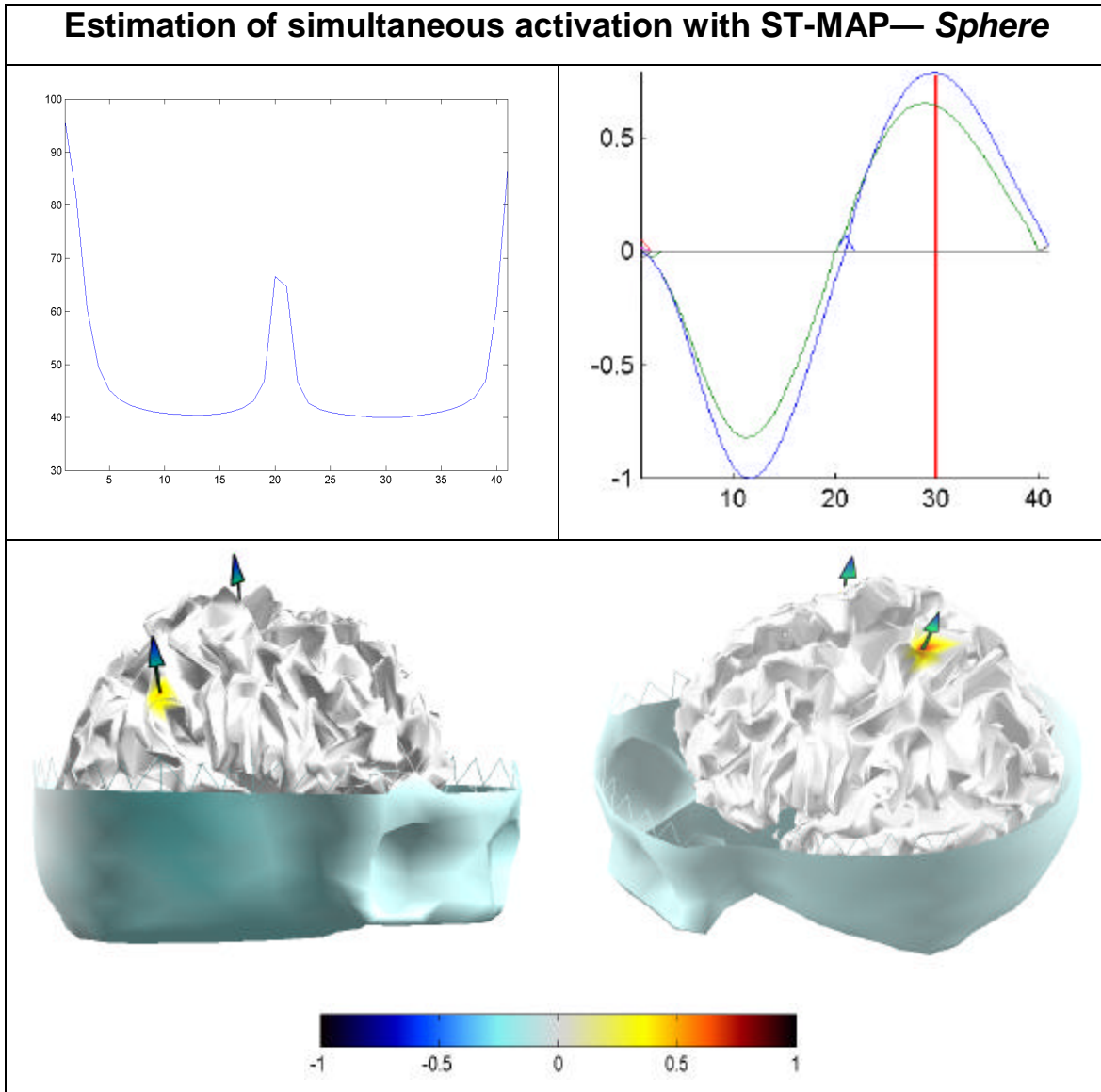


Figure 19 — The results from ST-MAP estimation of synchronous activity with the Sphere model.

Conclusion

Some more sophisticated source model has been introduced owing to the design of a weighted neighborhood system on the pseudo-cortical surface that has been fitted to the phantom-head geometry. This prior information has been introduced in the model of the source distribution for resolution of the inverse problem with a non-linear estimator of the source amplitudes, ST-MAP. We have adapted the original ST-MAP algorithm into a recursive focusing procedure to iteratively reduce the dimension of the source space.

This method gives satisfactory results when single focal activity is present, except in the case of deeper source, where the SNR is too weak. Without considering this kind of sources, the *FEManiso* model allows the best accuracy in the source localization, whereas the other head models with realistic geometry (*FEManiso_TR*, *FEMiso*, and *BEM*) may introduce some very little localization bias. The *Sphere* model gives equivalent results to *FEManiso*'s. Indeed, the analytical formulation of the forward problem introduces no numerical perturbations in its solution and thus produces better conditioned gain matrices \mathbf{G} that compensates for the lost in the geometry and conductivity parameters. Nevertheless, the higher residual rates of the sphere source models may be practically intractable to interpret real data sets.

Finally, simple synchronous source activation patterns can also be properly recovered using both the *FEManiso* and the *Sphere* model.

We should also insist on the importance of the temporal regularization term that plays an essential role in the preservation of the source time courses at the zero-crossing potentials. This temporal constraint goes further than the simple initialization of the iterative estimates by the previous source estimation. Using this latter may make errors propagate along the following iterations. The time constraint used here behaves in a more flexible way with fine balancing with the spatial regularization priors.

As a conclusion, some proper regularization scheme can help for the recovery of the original source pattern, in the case of the very simple activation design that have been adopted for the phantom head sources.

It is also important to note that the good performances from the *Sphere* model descend from the fact that there was no source in the frontal regions of the simulated cortex. In these areas, discrepancies between the true anatomy and its spherical simplification are much more important than for the rest of the skull. Some degradation in the performances of reconstruction procedures with the *Sphere* for such sources has been noticed in (Leahy *et al.* 1998) in a similar experiment.

4. DISCUSSION AND CONCLUSIONS

We have investigated in which way the accuracy of typical techniques for the resolution of the inverse problem in EEG is sensitive to characteristics of the head model. These include the model for head geometry (which could be spherical or realistic), the spatial sampling of the head compartments (piece-wise homogeneous descriptions with surfacic meshes or concentric sphere models; volumic meshes using FEM), and the conductivity properties of the head tissues (with the possibility to take anisotropy and inhomogeneity into account with the FEM approach). Previous studies have investigated the sensitivity of solutions to the forward problem to changes in the head geometry and the conductivity parameters of the tissues (see for instance Meijs *et al.* 1989, Haueisen *et al.* 1995, Marin *et al.* 1998). It appeared that little changes in those parameters would have dramatic consequences in the estimation of the potentials on the scalp. Thus, these studies tended to state that the use of realistic head models, possibly with anisotropy properties included, would be indispensable for correct estimation of the underlying cortical sources.

In this present study, we have evaluated the robustness of typical inverse techniques toward modeling errors or simplifications in the forward solutions. In other words, to which extent is it possible to properly estimate the underlying activity despite an imperfect head model?

For this study, it appeared that simulated data recordings using a real skull phantom head would be a better, *i.e.* more realistic, approach than common numerical simulations. These latter can not take completely into account all the possible perturbations occurring in true data acquisition such as the environment noise and noise in electronics. Further, it is not straightforward to model exactly the deformations of volume currents when passing through the skull bone. Previous studies using MEG have used a plastic phantom head for such investigations. However, similar works in EEG necessitate the use of a real skull head.

Following early works in (Cohen *et al.* 1990) and (Greenblatt and Robinson 1994) (see section 1), we have used a real skull phantom head very similar to the one used in (Leahy *et al.* 1998). But here, we have deeply investigated the respective merits of typical inverse techniques working together with different head models.

4.1 SPATIO-TEMPORAL DIPOLE FIT AND THE BESA IMPLEMENTATION:

We have used here the best spherical head model using the projections of the true electrode locations after 3D registration. Further, the conductivity parameters have been set to the average values measured on the true phantom tissues (Baillet *et al.* 1997). The BESA user knew *a priori* the exact source positions and how many sources were active at the same time.

If the Residual Variance criteria was used as the only parameter in the non-linear fit cost function, sources could not be recovered properly with errors of more than $3cm$. This is explained by errors in the forward solution from the sphere model. If RV is the only fit criterion, then the algorithm will tend to fit at its best the sensors with higher SNR with the systematic bias of the sphere head model, and without considering the whole EEG scalp topography in the source fit. To decrease the RV rate, this is a common practice to introduce a supplementary source in the model. Then RV decreases substantially but spurious sources appear, usually located at some distance of the true source location and with significant magnitude; producing dipole models very difficult to interpret because it is not clear how to discriminate true sources from spurious ones.

Instead, the user tuned the fit criteria of the non-linear cost function (like the *variance* and *separation* criteria) as supplementary priors to the source estimation. Then, localization accuracy on the order of $1cm$ can be achieved, which is very consistent with results in (Leahy *et al.*, 1998), but with high RV rates (from 6% to 71 %, typically 20%).

As a conclusion, the BESA approach can give key information to the experimenter if great care is adopted in the interpretation of dipole time courses and comparison of true EEG scalp maps with the ones produced by the solution. In that sense, careful tuning of the fit criteria should be done in accordance with the current dipole model. And more precisely, RV is a quantitative index that should play a minor role in the interpretation of the source model in comparison with EEG scalp topography and the evaluation of possible interaction between dipoles.

4.2 DISTRIBUTED SOURCE MODELS IN THE WHOLE HEAD VOLUME

The LORETA source estimates work in the entire inner volume of the head. The source space is sampled according to a regular grid of voxel. Each grid point corresponds to a regional source made of 3 orthogonal dipoles. The LORETA priors correspond to a smooth distribution of the source intensities in the entire source space.

Such priors are not well suited to the estimation of focal sources. That is the main reason why both some large localization errors and spurious activity appeared in our source estimates with LORETA.

Some possible solution would be to refine the original source grid and/or to apply source space restriction using either or both:

Focusing methods like the VARETA variation of LORETA (Valdes-Sosa *et al.*, 1996)

Restriction on the cortical surface with dense spatial sampling.

Both of these are currently under investigation in our groups.

4.3 DISTRIBUTED SOURCE MODELS ON THE CORTICAL SURFACE

More constraints in the source reconstruction have been introduced by fitting a true cortical surface in the phantom head, and applying inverse methods that work on the restricted cortical anatomy.

4.3.1 SOURCE ESTIMATION WITH MINIMUM NORM CONSTRAINTS

This method introduce prior information in the source model that is not well suited to source estimation. And indeed, for both the *FEManiso* and the *Sphere* model, the reconstruction results have strong localization bias and high rate of spurious source activity, thus producing source image impossible to interpret properly.

4.3.2 RECURSIVE SOURCE ESTIMATION WITH MINIMUM NORM CONSTRAINTS, FOCUSS

This method possesses a prior source model, which is very well suited to focal source estimation.

Some of the dipoles are properly located, but there is some important bias on the localization of the deeper source S4, and smaller one for S2 (about $1cm$) and S3 ($2cm$) with both *FEManiso* and *Sphere* head models.

Synchronous source firings can be recovered, but with noise sensitivity to zero-crossing potentials (where SNR is very low), and the appearance of limited spurious activity with the *Sphere* model.

The FOCUSS method, because of the good fit of its source model to the present data set brings major improvement to classical MNE. However, some uncertainties in source location or distributed source activities still remain for some of the source arrangements.

4.3.3 NON LINEAR SOURCE ESTIMATION WITH MODIFIED ST-MAP

The last method we have been using is a modified version of the ST-MAP method for distributed source pattern estimation. When the spatial sampling of the source space is too sparse (*i.e.* there are too few source locations to properly sample the cortex geometry), the underlying source activity may be considered as focal. We have developed a modified version of the ST-MAP method for focal source estimation by iterative reduction of the dimension of the source space.

Deeper source S4 is still not properly located (localization error $> 1cm$). It is very likely that SNR here was too low for proper source estimation.

The other sources are perfectly located with the *FEManiso* model. Other realistic head models make some limited bias appear ($< .4cm$) on deeper source S2. Synchronous firings are well estimated with both the *FEManiso* and the *Sphere* models.

The *Sphere* head model produces similar results as *FEManiso*'s. As analytical solution to the forward problem produce better-conditioned gain matrices than numerical computations, the associated inverse problems are much easier to regularize with lesser sensitivity to the tuning of the regularization parameter. Another important point here is that

the phantom sources were not located in the frontal areas where the sphere approximation of the head geometry produces the worse model (see (Leahy *et al.* 1998)).

4.4 DISCUSSION

As a conclusion, and at first glance, this study seems to speak more in favor of greater efforts on source modeling than on head modeling. It means that if proper source models and regularization schemes are applied, then there is little gain in using a realistic head model in comparison with the sphere. However, these results are based on very simple firing patterns in the source space, namely focal source activity.

These findings should be considered as primary experimental steps, going further the usual numerical simulations, for the evaluation of the solutions of the inverse and forward problems. Further, in some cases like inter-ictal source localization in epilepsy due to tumors or lesions, it is likely that the multiple-focal source model may bring some interesting information to clinical interpretation and pre-surgery diagnostic (see for instance Diekmann *et al.* 1998). Some preliminary results using the current implementation of multi-focal ST-MAP for source analysis of inter-ictal activity in patients suffering from complex partial epilepsy has produced promising insight of the diversity of the brain structures involved (Baillet *et al.* 1998).

However, in a previous study (Marin *et al.* 1998) using numerical simulations, we have shown that anisotropy parameters are essential to the proper recovery of truly distributed source patterns. In the case of complex underlying source arrangements, focusing procedures such as those described herein will systematically fail, as they do not possess the proper source model as priors. Hence, these methods should not be considered as the most appropriate: even the most primary cortical activation is likely to involve **multiple and extended areas** with complex source arrangements along the cortical mantle (Rizzolatti *et al.* 1998, Alarcon *et al.* 1994).

Thus we strongly believe that if proper multi-resolution estimation methods, that go further current focusing techniques, are developed, then better accuracy could be reached with hopefully less sensitivity to the head model.

We are currently working at some necessary improvements to the ST-MAP procedure that will work on iterative multi-resolution procedures with increasing source densities for a

better spatial sampling of the cortical surface (Gavit *et al.* 1998). Actually, despite ST-MAP's decent performances on these data, it is obvious that the underlying focal source pattern is not adequate for a true evaluation of the possibilities offered by the sophisticated source model developed in our method. We think that further investigations with more complex (*i.e. more distributed*) source patterns generated inside the phantom head would help this kind of approach grow and improve.

A very last point that we consider of great interest, is the introduction of constraints in the time domain. Simple considerations as the ones introduced in ST-MAP help the algorithm to recover a gently varying time course for the source estimates. Further investigations in both data pre-processing to identify and isolate signal components of interests, and more complete temporal constraints, possibly on source dynamics (Le Van Quyen *et al.* 1997), would contribute to significant advances in the MEG-EEG source estimation techniques.

REFERENCES

- Alarcon, G./ Guy, C./ Walker, S./ Elwes, R./ Polkey, C. (1994)** , "Intracerebral propagation of interictal activity in partial epilepsy: implications for source localisation", *J. of Neurol., Neurosurgery and Psychiatry*, Vol. 57, pp. 435-449, 1994
- Baillet, S./ Garnero, L. (1997)** , "A Bayesian Approach to Introducing Anatomic-functional Priors in the EEG /MEG inverse problem", *IEEE Trans. on Biomed. Eng.*, Vol. 44, N°3, pp. 374-385, 1997
- Baillet, S./ Garnero, L./ Marin, G./ Hugonin, J.-P. (1998)** , "Combined MEG and EEG source imaging by minimization of mutual information", *submitted to IEEE Trans. on Biomed. Eng.*, 1998
- Baillet, S./ Marin, G./ Le Rudullier, F./ Garnero Line (1997)** , "Evoked potentials from a real skull phantom-head: An experimental step to the validation of methods for solving the forward and inverse problems of brain cortical imaging", *Human Brain Map.*, *submitted*, 1997
- Barth, D./ Sutherling, W./ Broffman, J./ Beatty, J. (1986)** , "Magnetic localization of a dipolar current source in a sphere and a human cranium", *Electroenceph. Clin. Neurophysiol.*, Vol. 63, pp. 260-273, 1986
- Blake, A./ Zisserman A (1987)** , "Visual Reconstruction", MIT Press, Cambridge: MA, 1987
- Charbonnier, P./ Blanc-Féraud, L./ Barlaud, M. (1996)** , "Deterministic edge-preserving regularization in computer imaging", *IEEE Trans. on Image Processing*, Vol. 5, N°12, 1996
- Cohen, D./ Cuffin, N. B./ Yunokuchi, K./ Maniewski, R./ Purcell, C./ Cosgrove, G./ Ives, J./ Kennedy, J./ Schomer, D. (1990)** , "MEG versus EEG localization test using implanted sources in the human brain", *Ann. Neurol.*, Vol. 28, pp. 811-817, 1990
- Cuffin, N. B. (1990)** , "Effects of head shape on EEG's and MEG's", *IEEE Trans. on Biomed. Eng.*, Vol. 37, 1990
- Dale, A./ Sereno, M. (1993)** , "Improved localization of cortical activity by combining EEG and MEG with MRI surface reconstruction: a linear approach", *J. Cogni. Neurosci.*, Vol. 5, pp. 162-176, 1993
- de Munck, J. (1988)** , "The potential distribution in a layered spheroidal volume conductor", *J. Appl. Phys.*, Vol. 64, pp. 464-470, 1988
- Demoment, G. (1989)** , "Image reconstruction and restoration: overview of common estimation structures and problems", *IEEE Trans. Acoust. Speech Signal Proces.*, Vol. 37, pp. 2024-2036, 1989
- Ebersole, J. S. (1994)** , "Non invasive localization of the epileptogenic focus by EEG dipole modeling", *Acta Neurol. Scand.*, pp. 20-28, *suppl. 152*, 1994
- Gavit, L./ Baillet, S./ Garnero, L. (1998)** , "Mise en oeuvre d'une approche multirésolution d'un estimateur non linéaire des sources de l'EEG et de la MEG", *Technical Report CNRS UPR 640 TIC 02*, 1998
- Geman, D./ Reynolds, G. (1992)** , "Constrained restoration and the recovery of discontinuities", *IEEE Trans. on Pattern Anal. Mach. Intell.*, Vol. 14, N°3, pp. 367-383, 1992
- Geman, D./ Reynolds, G. ,** "Constrained restoration and the recovery of discontinuities", *IEEE Trans. on Pattern Anal. Mach. Intell.*
- Geman, S./ Geman Donald (1984)** , "Stochastic relaxation, Gibbs distributions and the Bayesian restoration of images", *IEEE Trans. on Pattern Anal.*, Vol. PAMI-6, pp. 721-741, 1984
- Geman, S./ Mac Clure, D. (1987)** , "Statistical methods for tomographic image reconstruction", *Inverse Problems*, Vol. 21, pp. 5-21, 1987

- Gevins, A. (1998)** , "The future of electroencephalography in assessing neurocognitive functioning", *Electroenceph. Clin. Neurophysiol.*, Vol. 106, pp. 165-172, 1998
- Gindi, G./ et al. (1993)** , "Bayesian reconstruction of functional images using anatomical information as priors", *IEEE Trans. on Biomed. Eng.*, Vol. 12, pp. 670-680, 1993
- Gloor, P. (1985)** , "Neuronal generators and the problem of localization in electroencephalography: application of volume conductor theory to electroencephalography", *Jour. of Clin. Neurophysiol.*, Vol. 2, pp. 327-354, 1985
- Golub, G. H./ Van Loan, C. F. (1983)** , "Matrix Computation", John Hopkins University Press, Baltimore, 1983
- Gorodnistky, I. F./ George, J. S./ Rao, B. D. (1995)** , "Neuromagnetic imaging with FOCUSS: a recursive weighted minimum norm algorithm", *Electroenceph. Clin. Neurophysiol.*, Vol. 95, pp. 231-251, 1995
- Greenblatt, R. E./ Robinson, S. E. (1994)** , "A simple head shape approximation for the 3 shell model", *Brain Topog.*, Vol. 4, pp. 331, 1994
- Hämäläinen, M./ et al. (1993)** , "Magnetoencephalography. Theory, instrumentation and applications to the noninvasive study of human brain function", *Rev. Modern Phys.*, Vol. 65, 1993
- Haneishi, H./ Ohyama, N./ Sekihara, K./ Honda, T. (1994)** , "Multiple current dipole estimation using simulated annealing", *IEEE Trans. on Biomed. Eng.*, Vol. 41, N°11, pp. 1004-1009, 1994
- Haueisen, J./ et al. (1995)** , "On the influence of volume currents and extended sources on neuromagnetic fields: a simulation study", *Annals of Biomed. Eng.*, Vol. 2, pp. 728-739, 1995
- Huang, M./ Aine, C./ Supek, S./ Best, E./ Ranken, D./ Flynn, E. (1998)** , "Multi-start downhill simplex method for spatio-temporal source localization in magnetoencephalography", *Electroenceph. Clin. Neurophysiol.*, Vol. 108, pp. 32-44, 1998
- Khosla, D./ Singh, M./ Don, M. (1997)** , "Spatio-temporal EEG source localization using simulated annealing", *IEEE Trans. on Biomed. Eng.*, Vol. 44, N°4, pp. 1075-1091, 1997
- Le Van Quyen, M./ Adam, C. L. J.-P. / Martinerie, J./ Baulac, M./ Renault, B./ Varela, F. (1997)** , "Temporal patterns in human epileptic activity are modulated by perceptual discrimination", *Neuroreport*, Vol. 8, pp. 1703-1710, 1997
- Leahy, R. M./ Mosher, J. C./ Spencer, M./ Huang, M. L. J. D. (1998)** , "A study of dipole localization accuracy for MEG and EEG using a human skull phantom", *Los Alamos Tech. Report N° LA-UR-98-1442*, 1998
- Lewine, J. D./ Edgar, J./ Repa, K./ Paulson, K./ Asture, R./ Orrison, W. (1985)** , "A physical phantom for simulating the impact of pathology on magnetic source imaging", *Biomagnetism: Fundamental Research & Clinical Applications*, Pergamon, New York, pp. 368-372
- Mangin, J.-F./ Frouin, V./ Bloch, I./ Régis, J./ Lopez-Krahe, J. (1995)** , "From 3D Magnetic Resonance Images to structural representations of the cortex topography using topology preserving deformations", *J. of Math. Imag. and Vision*, Vol. 5, N°4, pp. 297-318, 1995
- Marin, G./ Guérin, C./ Baillet, S./ Garnero, L. M. G. (1998)** , "Influence of skull anisotropy for the forward and inverse problem in EEG : simulation studies using FEM on realistic head models", *Human Brain Map.*, in press, 1998
- Marquardt, D. W. (1963)** , "An algorithm for least-squares estimation of non-linear parameters", *J. Soc. Indust. Appl. Math.*, Vol. 11, pp. 431-441, 1963

- Matsuura, K./ Okabe, Y. (1995)** , "Selective minimum-norm solution of the biomagnetic inverse problem", *IEEE Trans. on Biomed. Eng.*, Vol. 8, N°44, pp. 608-615, 1995
- Meijs, JW. (1989)** , "On the numerical accuracy of the Boundary Element Method", *IEEE Trans. on Biomed. Eng.*, Vol. 36, 1989
- Menninghaus, E./ Lütkenhönher, B./ Gonzalez, S. L. (1994)** , "Localization of a dipolar source in a skull phantom: realistic versus spherical model", *IEEE Trans. on Biomed. Eng.*, Vol. 41, N° 10, pp. 986-989, 1994
- Miltner, W./ Braun C./ Johnson Jr., R./ Simpson, G./ Ruchkin, D. (1994)** , "A test of brain electrical source analysis (BESA): a simulation study", *Electroenceph. Clin. Neurophysiol.*, Vol. 91, pp. 295-310, 1994
- Mosher, J. C./ Leahy Richard M. (1998)** , "Source localization using recursively applied and projected (RAP) MUSIC", *Los Alamos Tech. Report N° LA-UR-98-1467*, 1998
- Nunez, P. L. (1981)** , "Electric fields of the brain", Oxford University Press, New York
- Okada, Y. (1983)** , "Neurogenesis of evoked magnetic fields", *Biomagnetism, an interdisciplinary approach*, Plenum, New-York
- Pascual-Marqui, R. M./ Michel, C./ Lehman, D. (1994)** , "Low resolution electromagnetic tomography: a new method for localizing electrical activity in the brain", *Int. Jour. of Psychophysiol.*, Vol. 18, pp. 49-65, 1994
- Peters, M. J./ de Munck, J. (1990)** , "The influence of model parameters on the inverse solution based on MEGs and EEGs", *Acta Oto-Laryngologica*, Scand. Univ. Press, pp. 61-69, *supp. 49*, 1990
- Phillips, J. W./ Leahy, R. M./ Mosher, J. C. (1997)** , "MEG-based imaging of focal neuronal current sources", *IEEE Trans. on Biomed. Eng.*, Vol. 16, N°11, pp. 338-348, 1997
- Radhakrishna Rao, C./ Kumar Mitra, S. (1973)** , "Theory and application of constrained inverse of matrices", *SIAM J. Appl. Math.*, Vol. 24, N°4, pp. 473-488, 1973
- Régis, J./ Mangin, J.-F. / Frouin, V./ Sastre, F./ Peragut, J.-C. / Samson, Y. (1995)** , "Generic model for the localization of the cerebral cortex and preoperative multimodal integration in epilepsy surgery", *Stereotactic and Functional Neurosurgery*, Vol. 65, pp. 72-80, 1995
- Riera, J. J./ Aubert, E./ Valdes P./ Casanova, R./ Lins, O. (1996)** , "Discrete spline electric-magnetic tomography (DSPET) based on realistic neuroanatomy", *Proceedings of the tenth Int. Conf. on Biomag. Biomag 96*, Springer-Verlag, *in press*, 1996
- Rizzolatti, G./ Luppino, G./ Matelli, M. (1998)** , "The organization of the cortical motor system: new concepts", *Electroenceph. Clin. Neurophysiol.*, Vol. 106, pp. 283-296, 1998
- Robillard, P./ Poussart, Y. (1977)** , "Specific-impedance measurements of brain tissues", *Med. & Biol. Eng. & Comput.*, Vol. 15, pp. 438-445, 1977
- Roland, P./ Geyer, S./ Amunts, K./ Schorman, T./ Schleicher, A./ Malikovic, A./ Zilles, K. (1997)** , "Cytoarchitectural maps of the human brain in standard anatomical space", *Human Brain Map.*, Vol. 5, pp. 222-227, 1997
- Rush, S./ Driscoll, D. A. (1968)** , "Current distribution in the brain from surface electrodes", *Anesthesia and analgesia, current researches*, Vol. 47, pp. 717-723, 1968
- Sarvas, J. (1987)** , "Basis mathematic and electromagnetic concepts of the biomagnetic inverse problem", *Phys. Med. Biol.*, Vol. 32, N°1, pp. 11-22, 1987
- Scherg, M./ Von Cramon, D. (1986)** , "Evoked dipole source potentials of the human auditory cortex", *Electroenceph. Clin. Neurophysiol.*, Vol. 65, pp. 344-360, 1986

- Snyder, A. Z. (1991)** , "Dipole source localization of brain electrical activity", *Electroenceph. Clin. Neurophysiol.*, Vol. 80, pp. 321-325, 1991
- Tarantola, A. (1987)** , "Inverse problem theory", Elsevier, New York
- Thévenet, M. (1992)** , "Modélisation de l'activité électrique cérébrale par la méthode des éléments finis", *Thèse INSA Lyon*, N°92 ISAL 0036, 1992
- Thévenet, M./ Bertrand, O./ Perrin, F./ Dumont, T./ Pernier, J. (1991)** , "The finite element method for a realistic head model of electrical brain activity", *Clin. Phys. Physiol. Meas.*, Vol. 12., pp. supp. A, 89-94, 1991
- Tikhonov, A./ Arsenin, V. (1977)** , "Solutions to ill-posed problems", Winston, Washington DC
- Valdes-Sosa, P./ Marti, F./ Garcia, F./ Casanova, R. (1996)** , "Variable resolution electric-magnetic tomography", *Proceedings of the tenth Int. Conf. on Biomag. Biomag 96*, Springer-Verlag, *in press*, 1996
- Valdes-Sosa, P./ Riera, J. J./ Casanova R. (1996)** , "Spatio-temporal distributed inverse solutions", *Proceedings of the tenth Int. Conf. on Biomag. Biomag 96*, Springer-Verlag, *in press*, 1996
- Varah, J. (1973)** , "On the numerical solution of ill-conditioned linear systems with applications to ill-posed problems", *SIAM J. Numer. Anal.*, Vol. 10, N°2, pp. 257-267, 1973
- Wikswo Jr, J./ Gevins, A./ Williamson, S. J. (1993)** , "The future of EEG and MEG", *Electroenceph. Clin. Neurophysiol.*, Vol. 87, pp. 1-9, 1993
- Yvert, B./ Bertrand, O./ Thévenet, M./ Echallier, J./ Pernier, J. (1997)** , "A systematic evaluation of the spherical model accuracy in EEG dipole localization", *Electroenceph. Clin. Neurophysiol.*, Vol. 102, pp. 452-459, 1997